ORDCIT Project
Contract No. W-04-200-ORD-455
ORDNANCE DEPARTMENT

Progress Report No. 4-103

EXPERIMENTAL STUDY OF GAS-FLOW SEPARATION IN OVEREXPANDED EXHAUST NOZZLES FOR ROCKET MOTORS

Charles R. Foster
Frederick B. Cowles

Nathaniel Van De Verg

Nathaniel Van De Verg, Chief
Liquid Rockets Section

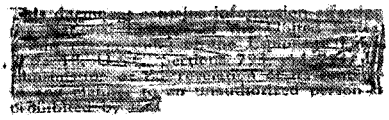

Louis G. Dunn

Louis G. Dunn, Director
Jet Propulsion Laboratory

Clark B. Millikan

Clark B. Millikan, Chairman
Jet Propulsion Laboratory Board

Copy No._____

50 P

JET PROPULSION LABORATORY
California Institute of Technology
Pasadena, California
May 9, 1949

TABLE OF CONTENTS

LIST OF TABLES

LIST OF FIGURES

LIST OF FIGURES (Cont'd)

LIST OF FIGURES (Cont'd)

I. INTRODUCTION AND SUMMARY

In a rocket motor having a de Laval nozzle with a fixed expansion ratio, there is only one pressure ratio[1] p_c/p_o for which this expansion ratio is correct. At any other pressure ratio the gases will be either underexpanded or overexpanded, depending on whether the pressure ratio is higher or lower than the correct value. Rocket motor flame patterns illustrating the four possible regimes are shown in Figures 1 to 4, inclusive. In Figure 1, the pressure ratio is higher than the correct one for the fixed expansion ratio of the nozzle, resulting in underexpansion of the gases. In Figure 2, the pressure ratio is the correct one. In Figure 3, the pressure ratio is only slightly lower than the correct one, resulting in overexpansion without separation of the gases from the wall. In Figure 4, the pressure ratio is considerably below the correct one, resulting in overexpansion with separation of the gases from the nozzle wall. The present report is concerned primarily with this fourth type of flow, that is, overexpansion of the gases with separation of the flow from the wall. Such a situation exists in a rocket motor operating at a considerably lower altitude than that for which its exhaust nozzle was designed.

Tests were made with overexpanded nozzles, and a record was taken of the pressure variation along the wall of the nozzle in each test.[2] The pressure followed the theoretical adiabatic expansion curve down to the point of separation below atmospheric pressure, and then returned quite abruptly to approximately atmospheric pressure. The point of separation was found to move downstream with increasing chamber pressure, the curve of separation area ratio vs chamber pressure being nearly a straight-line function. Typical values are: separation at area ratio 5.5 at 200 psia chamber pressure, and separation at area ratio 8.3 at 350 psia chamber pressure. Also the point of separation was found to be relatively unaffected by changes in the nozzle divergence angle, varying only about 0.8 area ratio at a given chamber pressure for changes in nozzle divergence half-angles from 10 to 30°.

The gases were found to separate from the wall when they had expanded to a pressure of about 5 psia, and this separation pressure decreased slightly with increasing chamber pressure. Of special significance is the fact that this separation pressure appears to be independent of mixture ratio, gas temperature, adiabatic expansion exponent γ (and hence propellant combination), total expansion ratio, and nozzle divergence half-angle.

The loss in thrust resulting from operation of a nozzle having a total expansion ratio of 10, as compared with one having a total expansion ratio of 3.65, was determined for various divergence half-angles. A typical experimental loss value was 8 per cent, compared with a theoretically predicted value of 12 per cent when separation was neglected.

---

[1] The nomenclature used in this report is given in Table I.

[2] Some preliminary tests with an overexpanded nozzle were made by R. B. Canright of this Laboratory, which aided materially in determining the course of the research reported herein.

II. TEST EQUIPMENT

A rocket motor having a nominal thrust of 750 pounds at 300 psia chamber pressure was used as the test motor. A drawing of this motor is shown in Figure 5. The injector used in all tests was the impinging-jet type with six pairs of replaceable orifices. Chamber pressure was measured at the injector face through a tap not shown in the drawing. The steel chamber and the chrome-plated copper nozzle were separately cooled by water. The cooling water was piped through Fischer-Porter rotameters for flow measurement, and temperature of the water was taken at each inlet and outlet by means of iron-constantan thermocouples. The millivolt output from these thermocouples was recorded on either a Brown or a Leeds and Northrup 12-point recording potentiometer.

The nozzle shown in Figure 5 was designed for optimum expansion, that is, for expansion from 300 psia chamber pressure to 14 psia atmospheric pressure at the nozzle exit. Drawings of the overexpanded nozzles tested are shown in Figure 6. These nozzles included three having expansion ratios of 10 with divergence half-angles of 10, 15, and 20°, and one having an expansion ratio of 20.8 with a divergence half-angle of 15°. The nozzle was water-cooled except for the portion between area ratio 3 and the exit, this portion of the expansion section being uncooled. This type of construction was possible because the temperature of the exhaust gases was low enough to prevent overheating of the uncooled portion beyond area ratio 3. This construction also greatly simplified the installation of the pressure taps for the pressure measurements. Holes of 1/32-inch diameter were drilled at 1/2-inch intervals in the expanding portion of the nozzle, starting at approximately area ratio 3 and extending to the nozzle exit. These holes were drilled carefully to be normal to the nozzle surface and to have sharp corners without burrs. The pressure was conducted to the mercury manometer bank through copper tubes, 1/4 inch in diameter, which were brazed into the nozzle wall as shown in Figure 6. Certain of the pressure taps were repeated in two other circumferential locations around the nozzle in order that any nonsymmetry of pressure might be determined. Figure 7 is a photograph of a typical nozzle showing all these details of construction. In this photograph, the cooled copper portion of the nozzle appears in the center, the outer case for optimum expansion is at the left, and the outer case for overexpansion is at the right.

The test rocket motor was mounted on a parallelogram-type thrust stand as shown in the photograph of Figure 8. The parallelogram was supported by eight ball bearings and pushed against a hydraulic piston (area 1 sq in.) for transmission of the thrust force to the recording gage. The hydraulic piston was rotated slowly within its housing in order to minimize friction forces. Operation of the rocket motor was observed through the windows between the control room and the concrete test area.

III. INSTRUMENTATION

The quantities of most importance to be measured during a test were thrust, chamber pressure, and pressures at the various stations in the expanding portion of the nozzle. Additional data taken but considered of minor importance were flow of oxidizer, flow of fuel, flow of cooling water through the chamber and nozzle, and temperature rise of this cooling water.

In order to increase the readability of the thrust measurement on the recording gage, a mechanical preload was applied to the thrust system. Known weights were placed in the preload pan on its lever arm, visible in Figure 8 just under the rocket motor, and acting in the direction opposite to that of the thrust force. The preload force could be varied by changing the weights in the preload pan; thus a thrust of 500 to 1000 pounds was always measured on a 250-pound gage. The instrument used was a Brown

circular chart-recording pressure gage, having a range of 0 to 250 psi. A similar gage, having a range of 0 to 500 psi, was used to obtain the chamber pressure record. The two circular chart-recording gages appear at the top of the control panel in Figure 9. Typical thrust and chamber pressure records obtained on these gages are shown in Figure 10. In this Figure, a portion of each of the circular charts has been reproduced. Note that, in this particular test, a preload of 426 pounds was used; the total thrust is therefore the chart reading plus 426 pounds. The chamber pressure was 235 psig (or 249 psia).

Pressures from the taps in the expanding portion of the exhaust nozzle were transmitted to the mercury manometer bank shown in Figure 9. There were twenty-six tubes in this bank. The black inch marks visible in the photograph were a great help in reading the mercury level in the various tubes. The manometer was illuminated from the rear in order that good pictures could be obtained. Pictures of the manometer bank were taken at frequent intervals during the tests. A means was provided for blowing out the tubes leading to the manometer bank, the twenty-six valves at the left in Figure 9 being used for this purpose. The tubes were blown out just before each test in order to remove any moisture condensation.

For propellant flow measurement, the depth of each propellant in its calibrated tank was measured before and after each test. The flow rate of the propellant was then obtained by dividing the quantity of propellant used by the duration of the test. The cooling water for the rocket chamber and nozzle was metered through Fischer-Porter rotameters. These rotameters were the visual type, giving a direct reading of the flow of water in pounds per second.

IV. TEST PROCEDURE

The test cell was piped according to the simplified diagram shown in Figure 11. The propellant tanks, containing red fuming nitric acid (6% NO_2 added) and aniline, were equally pressurized from commercial high-pressure nitrogen cylinders through a pressure-reducing regulator. Opening the first set of valves in the propellant lines established flow through the restrictors in the starting circuit. The ignition of red fuming nitric acid and aniline in the rocket motor is spontaneous. The chamber pressure developed by this restricted flow acted on a pressure switch which in turn opened the second set of valves in the propellant lines, establishing the flow through the full-flow circuit. With this method of operation, test starts were obtained quickly and were nearly identical from test to test.

Tests were normally 30 seconds in duration, and in those tests made with over-expanded nozzles, pictures were taken of the manometer bank recording the nozzle pressures at 1- or 2-second intervals. From these manometer pictures it was determined that equilibrium conditions were reached in approximately 5 seconds, and pressures were relatively steady after that interval.

V. RESULTS OF TESTS

The exhaust nozzle for a rocket motor normally has a much larger divergence angle than is usual in the design of the de Laval steam nozzle. The advantage of increasing the nozzle divergence angle is the reduction in the weight of the nozzle and in the surface area of the nozzle through which heat losses occur. The disadvantage is, of course, a loss in thrust. Early experiments at this Laboratory indicated that a divergence half-angle of 15° was a good compromise when these factors were considered, and nozzles having approximately this divergence angle have been used since that time.

In the present series of tests, a nozzle having a divergence half-angle of 15° was tested first. Subsequently, nozzles having divergence half-angles of 10 and 20°

were tested, since it was believed that this range would cover the normal spread encountered in rocket motor work. Finally, because an apparently anomalous result was obtained, a nozzle having a divergence half-angle of 30° was tested.

A. Separation Data

1. *Method of presenting data.* Results of individual tests are presented by plotting the pressure ratio p_c/p against the area ratio f/f_t, where

p = pressure measured at plane in nozzle

f = area of nozzle cross section where pressure is p

p_c = chamber pressure

f_t = nozzle throat area

Included on each graph of the data are theoretical curves assuming adiabatic expansion of the gas through the nozzle according to the usual expression (Cf. Ref. 1):

$$\frac{f}{f_t} = \Gamma' \left\{ \gamma \left(\frac{p}{p_c}\right)^{\frac{1}{\gamma}} \left(\frac{2}{\gamma - 1}\right)^{\frac{1}{2}} \left[1 - \left(\frac{p}{p_c}\right)^{\frac{\gamma - 1}{\gamma}}\right]^{\frac{1}{2}} \right\}^{-1}$$

in which Γ' is a constant defined by the equation

$$\Gamma' = \gamma \left(\frac{2}{\gamma + 1}\right)^{\frac{\gamma + 1}{2(\gamma - 1)}}$$

Theoretical curves for $\gamma = 1.20$ and $\gamma = 1.26$ are included, since these values will approximately bracket conditions encountered in the acid-aniline rocket motor.

The results from groups of tests have been summarized in regard to separation data by plotting the chamber pressure against the area ratio at which separation occurred.

2. *Tests with nozzle of 15° divergence half-angle and at high mixture ratio.* Operation at a mixture ratio of approximately 3 produces maximum exhaust velocity with the acid-aniline propellant combination. However, at this mixture ratio, where the combustion temperature is 5020°F, the lifetime of some rocket motor parts (such as chrome-plated copper nozzles) is rather limited. For this reason, most tests were made at a mixture ratio of 1.9 to 2.0 (combustion temperature 3650°F), but a few tests were made at high mixture ratio to determine the effect of varying this parameter.

Three tests were made at mixture ratios of 3.1 to 3.3, and the data are plotted in Figures 12, 13, and 14. The nozzle had a divergence half-angle of 15° and a total expansion ratio of 10.0, and the tests were made at 302 to 306 psia chamber pressure. The experimental curve followed the theoretical adiabatic expansion curve down to the point of separation (which was considerably below atmospheric pressure) and then rose quite abruptly to approximately atmospheric pressure. Separation of the gas from the wall in these tests at high mixture ratio occurred at an area ratio of 8.0 to 8.1 where the static pressure was 5 psia.

Subsequent tests at lower mixture ratio showed that the experimental curve followed the theoretical adiabatic expansion curve of a correspondingly higher value of γ, as it should for a lower combustion temperature. In fact, in most tests, the

shape of the pressure curve upstream from the separation point fitted a theoretical adiabatic expansion curve closely enough to permit determination of the effective adiabatic exponent γ to a fair degree of accuracy. Thus, since the effect of changes in mixture ratio had been tested and found to be normal and predictable, the remaining tests were made at a mixture ratio of about 1.9 in order that the equipment would have a suitable lifetime.

3. *Tests with nozzle of 15° divergence half-angle at various chamber pressures.* With the nozzle having a total expansion ratio of 10.0 and a divergence half-angle of 15°, a systematic study of the effect of variations in chamber pressure was made. All of the tests were made at a mixture ratio of about 1.9. Results of the individual tests are shown in Figures 15 through 24, which are arranged in order of increasing chamber pressure. Separation of the gases from the wall occurred at every chamber pressure tested, with a rather abrupt return to near-atmospheric pressure just downstream from the separation point, and then a gradual return to exactly atmospheric pressure at the nozzle exit.

In several of these tests (Cf. Figs. 15, 16, 17, 19, 20, 23, and 24) a nozzle was used in which the pressure taps extended as far upstream as the throat of the nozzle. The purpose of these tests was to determine that no discontinuities existed in the expansion process at any place between the throat and the nozzle exit. That no discontinuities existed is evident from the smoothness of the curves plotted from the measurements taken. Within the experimental accuracy, the measured throat pressure agreed with the predicted value (Cf. Ref. 1) of

$$\frac{p_t}{p_c} = \left(\frac{2}{\gamma + 1}\right)^{\frac{\gamma}{\gamma - 1}}$$

A summary curve for the separation data is presented in Figure 25, in which the area ratio at the plane of separation is plotted against chamber pressure. From this curve it is seen that the point of separation moves downstream as the chamber pressure increases. The change is nearly a straight-line function, the point of separation varying from area ratio 5.5 at 200 psia chamber pressure to area ratio 8.3 at 350 psia chamber pressure.

As noted in Section II, on some of the nozzles certain pressure taps were repeated in two other circumferential locations around the nozzle in order that any nonsymmetry of pressure might be determined. During the tests, the pressures were found to be quite symmetrical, the greatest deviations occurring, as would be expected, in the pressure downstream from the plane of separation where the pressure curve was returning very steeply toward atmospheric pressure. The method of indicating the asymmetry of pressure is given in Figure 21. Here the dotted vertical line through alternate test points indicates the amount of asymmetry at the point, and the three circumferential pressures fall within these vertical lines. The only point of appreciable difference is at area ratio 7.55, which is just downstream from the separation plane. Because of the rapid rate of change of pressure in this region, this asymmetry is also negligible. In all subsequent graphs, vertical dotted lines through test points have the same meaning as indicated here.

4. *Tests with nozzle of 15° divergence half-angle and expansion ratio 20.8.* Tests were made with a nozzle having a total expansion ratio of 20.8 and a divergence half-angle of 15°. One purpose of these tests was to determine whether the length of

the nozzle affected the plane of separation of gases from the wall. Data from the individual tests are shown in Figures 26 through 31, which are arranged in order of increasing chamber pressure. The pressures were nearly identical with the pressures measured in the nozzle having a total expansion of 10, following the theoretical adiabatic expansion down to the point of gas separation and then returning to atmospheric pressure at the nozzle exit. Also the plane of separation of the gases was nearly identical, as indicated by Figure 32, in which the area ratio at the plane of gas separation is plotted against chamber pressure. The experimental points for both nozzles (ϵ = 10.0 and ϵ = 20.8) are shown in the Figure.

Although the plane of separation of the gases from the wall is not affected by the length of the nozzle, the thrust of the motor is less for the nozzle having a total expansion ϵ of 20.8 than for the nozzle having a total expansion ϵ of 10.0. The increased loss is due to the larger area of the nozzle downstream from the separation plane where the pressure inside the nozzle is subatmospheric. More details on this point will be given in Section V-C.

Another important result has been determined with this greatly overexpanded nozzle; the detached flow persists even when the chamber pressure is made sufficiently low to satisfy conditions for the occurrence of a plane shock wave within the nozzle. According to the rocket motor theory which neglects separation, the plane shock wave would stand at the exit plane of the nozzle when the pressure just upstream from the normal shock p_{s_1} and the chamber pressure are such (Cf. Ref. 2) that

$$\frac{p_o}{p_{s_1}} = \frac{4\gamma}{\gamma^2 - 1}\left[\left(\frac{p_c}{p_{s_1}}\right)^{\frac{\gamma - 1}{\gamma}} - 1\right] - \frac{\gamma - 1}{\gamma + 1}$$

and

$$\frac{f_e}{f_t} = \frac{\left(\frac{2}{\gamma + 1}\right)^{\frac{\gamma + 1}{2(\gamma - 1)}}}{\left(\frac{p_{s_1}}{p_c}\right)^{\frac{1}{\gamma}}\sqrt{\frac{2}{\gamma - 1}\left[1 - \left(\frac{p_{s_1}}{p_c}\right)^{\frac{\gamma - 1}{\gamma}}\right]}}$$

For any chamber pressure less than this value, the theory indicates that the shock wave would occur within the nozzle.

For the nozzle having a total expansion ratio of 20.8, the conditions for the normal shock to stand at the exit plane of the nozzle are satisfied when the chamber pressure is 197 psia. Tests were made with the nozzle at chamber pressures as low as 130 psia; separation continued to occur, with no indication of the normal shock at any chamber pressure between 130 and 200 psia. Figure 32 shows one point at 167 psia chamber pressure with gas separation occurring at expansion ratio 4.7.

Thus it has been demonstrated that, with a nozzle having a divergence half-angle of 15° and under the conditions of the tests, the plane shock wave solution postulated in such theories as Reference 2 does not occur.

5. *Tests with nozzles of 10, 20, and 30° divergence half-angles.* Rocket motor nozzles for most applications may be expected to have a divergence half-angle between

about 10 and 20°. In order to have complete data covering this range, tests were made with a nozzle having a divergence half-angle of 10° and also with one having a divergence half-angle of 20°. For each of these nozzles the total expansion ratio was 10.0, similar to the previous nozzle having a divergence half-angle of 15°.

Pressures measured during individual tests with a nozzle of 10° divergence half-angle are shown in Figures 33 through 36, which are arranged in order of increasing chamber pressure. Similarly, tests with a nozzle of 20° divergence half-angle are shown in Figures 37 through 42. The behavior in these nozzles was similar to that in the previous nozzles, pressure following approximately an adiabatic expansion curve to the point of separation and returning to atmospheric pressure at the nozzle exit.

A summary of the separation data for these two nozzles, as well as a repetition of the data for the nozzle of 15° divergence half-angle, is given in Figure 43. As shown, separation occurred in the 10 and 20° nozzles along curves parallel to the curve for the 15° nozzle, but at slightly larger area ratios for equal chamber pressures. The curve for the 20° nozzle fell between the curves for the 10 and 15° nozzles, and the small scatter of the data around these curves seemed to indicate that this effect was real.

Because of the apparently anomalous results mentioned in the previous paragraph, a nozzle having a divergence half-angle of 30° was constructed and tested in an effort to clear up this effect. Pressures measured during individual tests with the nozzle of 30° divergence half-angle are shown in Figures 44 through 48, which are arranged in order of increasing chamber pressure. The data did not have the same consistency as had been obtained with the previous nozzles, and when the separation data were plotted, as shown in Figure 49, the points scattered among the points for the other three nozzles.

The scatter obtained with the nozzle of 30° divergence half-angle was probably due to one, or a combination, of the following factors: (1) Tests for symmetry of separation made with the 20° nozzle (vertical dotted lines through points in Figs. 37 through 42) showed an increase in asymmetry of separation over that in the 10 and 15° nozzles. Tests for symmetry of separation were not made with the 30° nozzle, and it seems probable that there was a greatly increased amount of asymmetry of separation with the nozzle of such a large divergence angle. This factor would account for the scatter in the separation data, and is very likely the major contribution. (2) Another possible source of difficulty may be that 30° is approaching too closely the angle at which separation is caused by divergence, and may thus result in unstable pressures in the overexpanded portion. Separation of the gases from the wall is known to occur with a divergence half-angle somewhere between 30 and 40°.

Although testing the 30° nozzle did not in itself clear the apparently anomalous results obtained with the other nozzles, it showed an important result: The plane of separation is relatively unaffected by changes in the nozzle divergence angle. It is evident, for instance, that in Figure 49, at a chamber pressure of 300 psia, separation would occur at an area ratio between 7.4 and 8.2 for any nozzle divergence half-angle between 10 and 30°. For all practical applications, this range of divergence angles is more than adequate, and rocket performance with overexpanded nozzles can be quite accurately estimated from the data presented.

Another result, which is possibly the most important with regard to practical applications, is a crossplot, from all of the foregoing curves, of separation pressure vs chamber pressure. This plot is shown in Figure 50, which includes points at high mixture ratio, at low mixture ratio, with total expansion ratios of 10.0 and 20.8, and with nozzles having divergence half-angles of 10, 15, 20, and 30°. Although there is considerable scatter of the points, there is a definite trend indicating that the pressure at which separation of the gases from the wall of the nozzle occurs decreases

as chamber pressure increases. Since points are included from all the nozzles tested, this curve appears to be independent of mixture ratio, gas temperature, adiabatic expansion exponent γ (and therefore propellant combination), total expansion ratio, and nozzle divergence half-angle. The one question that could not be determined with the present experimental equipment was the effect of varying the back pressure. In all tests, the back pressure was atmospheric pressure of about 14.2 psia. If the influence of the absolute value of back pressure is not appreciable, the designer of a high-altitude rocket could assume adiabatic expansion of the gases from the chamber pressure to the pressure shown by Figure 50, at which pressure separation would take place; thus the designer could determine thrust at launching and during flight.

B. Induced Separation

For each external pressure there exists an optimum nozzle whose expansion ratio gives maximum thrust. For vertical flight, where pressure is continually decreasing, the most efficient nozzle would be one with a continually varying expansion ratio. Because of the evident difficulties of constructing such a nozzle, present-day rockets have a rigid nozzle designed for some mean altitude. In some instances, however, an appreciable increase in altitude might be obtained by having two or three expansion ratios built into one nozzle with a means for causing gas separation to change from one to another. It has been shown (Cf. Ref. 3) that, in most instances, very little advantage is obtained by having more than two such steps.

During the course of the present investigation, several possible methods of inducing separation at a desired area ratio have come to mind. (1) A ring (or rings) of holes (Cf. design *a* of Fig. 51) might be drilled in the nozzle wall and connected to external pressure or ram pressure of the ascending rocket, causing separation at the air inlet. These openings could be valved off as the rocket ascended and a larger nozzle area ratio was required. (2) An abrupt change in angle in the diverging portion of the nozzle wall (Cf. design *b* of Fig. 51) might cause separation at low pressure ratios of p_c/p_o and not at the higher pressure ratios at increased altitude. (3) A step (or steps) of material of proper melting temperature might be placed in the diverging portion of the nozzle to cause separation until each successive step was burned away (Cf. design *c* of Fig. 51). (4) A sliding section might be built into the nozzle that would move out into position at a predetermined pressure ratio (Cf. design *d* of Fig. 51).

A few preliminary tests have been made using the first of these methods, that is, drilling holes through the nozzle wall to allow air to be drawn in, thus causing separation. Six tests were made. A brief description of each test follows, and graphs of pressure ratio vs area ratio for each test are shown in Figures 52 through 57.

1. In test E40W (Cf. Fig. 52) the nozzle having a divergence half-angle of 15° and a total expansion ratio of 10.0 was used. First, fourteen holes of 1/4-inch diameter were drilled through the nozzle wall at area ratio 7.0. At a chamber pressure of 330 psia where separation would occur normally at area ratio 8.0, separation was induced at the air inlet holes at area ratio 7.0. Fluctuations in the pressure near the separation point are indicated by the dotted portion of the curve with the limits of fluctuation indicated by the two plotted points at area ratio 7.0.
2. In test E41W (Cf. Fig. 53), using the same configuration as in test E40W, a test was made at 350 psia chamber pressure where separation would occur normally at area ratio 8.3. Again, separation occurred at the air inlet holes at area ratio 7.0. Increased fluctuations in

pressure downstream from the separation point were noted.

3. In test E42W (Cf. Fig. 54) an effort was made to distribute the incoming air more evenly; the fourteen holes of 1/4-inch diameter were connected by a groove 3/32 inch wide and 1/8 inch deep on the inner surface of the nozzle. A test was made at 351 psia chamber pressure where separation would occur normally at area ratio 8.3. Separation occurred at the air inlet, and an appreciable decrease in the pressure fluctuations downstream from the separation point was obtained.
4. In test E44W (Cf. Fig. 55) a second ring of holes consisting of five holes of 1/4-inch diameter was drilled through the nozzle wall at area ratio 4.8 and connected by a groove 3/32 inch wide and 1/8 inch deep on the inner surface. The objective was to cause gas separation at this area ratio. A test was made at 328 psia chamber pressure where separation would occur normally at area ratio 8.0. Separation did not occur at the upstream air inlet at area ratio 4.8, but continued to occur at the second air inlet at area ratio 7.0.
5. In test E45W (Cf. Fig. 56), using the same configuration as in test E44W, a test was made at 255 psia chamber pressure, at which pressure the normal separation point is at area ratio 6.6. Separation did not occur at the upstream air inlet, but continued at the normal separation point.
6. In test E47W (Cf. Fig. 57), in order to simulate ram pressure in an actual vehicle, nitrogen gas at a velocity of 500 ft/sec was introduced at the upstream air inlet holes. This velocity was chosen since it is that of the existing *WAC CORPORAL* vehicle at the end of boost. With a chamber pressure of 308 psia (normal separation point area ratio 7.6) the gases still did not separate at the upstream air inlet, but continued to separate at the downstream air inlet at area ratio 7.0.

In this series of preliminary tests, a limited amount of success was obtained with this method of inducing separation of the gases from the rocket nozzle wall. For a specific application in which an appreciable advantage could be obtained by having more than one nozzle expansion ratio, additional tests with design *a* of Figure 51 (or one of the other three designs) would be warranted, with good chances for early successful achievement. Examples of the advantage that can be obtained by having a nozzle with two expansion ratios rather than one fixed expansion ratio have been calculated in Reference 3. A nozzle designed with an infinitely variable area ratio, such that the optimum may be obtained for each altitude, was chosen (Cf. Ref. 3) as the standard by which maximum performance may be calculated. The ratio of the summit altitude reached by a rocket vehicle with a conventional nozzle of fixed area ratio to the altitude obtained by the ideal nozzle is symbolized by the ratio R. In one example it is shown that, for a rocket vehicle having a sea-level specific impulse of 200 seconds, an initial acceleration of 1 g, and initial velocity of 0, a loading density of 0.85, a chamber pressure of 300 psia, and γ of 1.2, the optimum fixed expansion ratio is 7.5 and $R = 0.835$. Then if a two-step nozzle of expansion ratios 6 and 35 is substituted, all other conditions remaining the same, R is increased to 0.913. In other words, a 9 per cent increase in summit altitude is obtained by using a two-step nozzle having expansion ratios of 6 and 35 over the altitude reached by a single-step nozzle of expansion ratio 7.5. Similar increases in altitude are indicated in the other examples calculated in Reference 3.

C. Effect of Overexpansion on Thrust

The equation for thrust of a rocket motor may be written in the form (Cf. Ref. 1)

$$F = \lambda \dot{m} V_e + (p_e - p_o) f_e$$

The two terms in the right-hand member of the equation are referred to as velocity thrust and pressure thrust, respectively. If $p_e = p_o$, all the thrust is velocity thrust. If $p_e < p_o$, the gases are overexpanded and the pressure thrust is negative, although partially compensated by an increased velocity thrust. If $p_e > p_o$, the gases are underexpanded. Although the pressure thrust will then be positive, it will not compensate completely for loss in V_e caused by inadequate expansion. In the present report, the effects of overexpansion on thrust are correlated by means of the thrust coefficient C_F.

$$C_F = \frac{F}{p_c f_t} = \Gamma' \left\{ \frac{2}{\gamma - 1} \left[1 - \left(\frac{p_e}{p_c} \right)^{\frac{\gamma - 1}{\gamma}} \right] \right\}^{1/2} + \left(\frac{p_e - p_o}{p_c} \right) \frac{f_e}{f_t}$$

In a rocket motor nozzle, if the phenomenon of jet separation did not take place but the gases followed an adiabatic expansion process down to the nozzle exit, then the theoretical loss in thrust would be as shown in Figure 58 for a change in expansion ratio from 3.5 to 10.0. Here C_F has been plotted against p_c for $\epsilon = 3.5$ and $\epsilon = 10.0$, assuming $\gamma = 1.26$ and no loss due to nozzle divergence ($\lambda = 1.0$). The loss in thrust in changing from $\epsilon = 3.5$ to $\epsilon = 10.0$ varies from 24.4 per cent at $p_c = 200$ psia to 8.8 per cent at $p_c = 350$ psia. In an actual nozzle, jet separation does occur and the loss in thrust is not as great as the theory indicates. In Figure 59, experimental C_F values have been plotted against p_c for nozzles having expansion ratios of 3.5 and 10.0, each having a nozzle divergence half-angle of 15°. It is seen that the loss in thrust in changing from $\epsilon = 3.5$ to $\epsilon = 10.0$ amounts to approximately 9.2 per cent at $p_c = 200$ psia to 7.1 per cent at $p_c = 350$ psia. In Figures 60 and 61, similar data are presented for nozzles having divergence half-angles of 10 and 20°, respectively, although the number of experimental points with these nozzles is insufficient to establish the curves to the same degree of accuracy as the curve for the 15° nozzle.

In tests made with the nozzle having a total expansion ratio of 10.0, the loss in thrust can also be obtained by integrating the pressure forces acting on the nozzle between area ratios 3.5 and 10.0. This check method was used in several tests and, by means of a graphical integration, agreement within 1 per cent of the measured thrust was obtained.

When separation of the gases takes place in a nozzle, subatmospheric pressure exists in the nozzle from that point to the nozzle exit. Thus, when the nozzle having a total expansion of 20.8 was tested, the gases separated at the same area ratio as in the nozzle having a total expansion ratio of 10.0 (as shown in Section V-A of this report); the thrust, however, was somewhat decreased. This effect is shown in Figure 62 in which C_F is plotted against chamber pressure for the nozzles having $\epsilon = 3.5$, 10.0, and 20.8. The ideal theoretical curve ($\lambda = 1.0$) is included in Figure 62. Whereas the average thrust loss between $\epsilon = 3.5$ and $\epsilon = 10.0$ is about 8 per cent, the average loss between $\epsilon = 3.5$ and $\epsilon = 20.8$ is about 11 per cent.

A summary of the rocket motor performance data obtained during all tests is given in Table II. In examining this table, it should be remembered that the accuracy of thrust, chamber pressure, and C_F is good, but that the accuracy of mixture ratio, exhaust velocity, and specific impulse is only fair because of the tank deflection method of obtaining flow rates. The accuracy of these latter items also decreases as the duration of the test decreases because of the influence of end effects (starting and stopping transients).

VI. CONCLUSIONS

Although the phenomenon of jet detachment has been observed before, the systematic behavior of the point of separation with chamber pressure apparently has not been described in the literature on this subject. In Reference 3, a hypothesis for predicting the nature of these curves of pressure ratio vs area ratio was established. It was assumed in Reference 3 that the detachment of the jet was accompanied by an oblique shock wave near the nozzle wall, and that the angle and strength of the oblique shock corresponded to the wedge angle θ, by which the stream lines adjacent to the wall were deflected. The hypothetical flow structure is sketched in Figure 63. By means of one-dimensional supersonic nozzle theory and one-dimensional oblique shock theory (applicable to the local region near the wall), a system of equations was developed that could be solved for the area ratio of separation as a function of pressure ratio for various parametric values of the wedge angle θ. If the experimental data for various values of α and the theoretical data for various values of the wedge angle θ are both plotted on the same graph, as in Figure 64, it is found that the experimental curve for each nozzle is reasonably parallel to the family of theoretical curves for constant wedge angle. The assumption of a constant wedge angle of $18\pm3°$ would include all of the experimental data. An interesting conclusion is that, over the range of conditions tested, the wedge angle is almost independent of the nozzle divergence angle, and is relatively unaffected by changes in pressure ratio, gas temperature, adiabatic expansion exponent γ, and nozzle length.

Another conclusion which has been tentatively established is that the separation pressure is independent of mixture ratio, gas temperature, adiabatic expansion exponent γ (and hence propellant combination), total expansion ratio, and nozzle divergence angle. This conclusion will be checked by further experimentation already undertaken by this Laboratory, using nitrogen gas in a two-dimensional nozzle.[1]

Since jet separation is found to occur in highly overexpanded nozzles, the loss in thrust at launching of a sounding rocket is not as severe as the theory predicts when jet separation is neglected. Preliminary attempts to induce separation at a desired area ratio have met with some success, and the performance of a sounding rocket might be improved by inducing separation of the jet at two or more area ratios during the powered flight.

[1]Unpublished report on experiments with two-dimensional supersonic exhaust nozzles using nitrogen gas by John D. McKenney of this Laboratory.

TABLE I

NOMENCLATURE

c = effective exhaust velocity (ft/sec).

c^* = characteristic exhaust velocity (ft/sec).

C_F = thrust coefficient.

f = area (sq in.).

f_e = nozzle exit area (sq in.).

f_s = area at plane of separation (sq in.).

f_t = nozzle throat area (sq in.).

F = thrust (lb).

I_{sp} = specific impulse (lb sec/lb).

$\dot{m}$ = mass flow rate (lb/sec).

p = pressure (psia).

p_c = chamber pressure (psia).

p_e = pressure at nozzle exit (psia).

p_o = atmospheric pressure (psia).

p_s = pressure at plane of separation (psia).

p_{s_1} = pressure upstream from normal shock (psi).

p_t = pressure at nozzle throat (psia).

r = mixture ratio = w_o/w_f.

t = time (sec).

V_e = exhaust velocity parallel to axis (ft/sec).

w_f = fuel flow rate (lb/sec).

w_o = oxidizer flow rate (lb/sec).

α = nozzle divergence half-angle (°).

γ = ratio of specific heats.

$\epsilon = f_e/f_t$ = nozzle expansion ratio.

$$\Gamma' = \gamma \left(\frac{2}{\gamma + 1}\right)^{\frac{\gamma - 1}{2(\gamma - 1)}}$$

θ = wedge angle (°).

λ = nozzle divergence angle function.

TABLE II

ROCKET MOTOR PERFORMANCE DATA

Test No.	t (sec)	F (lb)	p_c (psia)	r	c^* (ft/sec)	C_F	I_{sp} (sec)	p_o (psia)	p_s (psia)	$\frac{f_s}{f_t}$
ϵ = 3.5 (Optimum); α = 15°										
32	30.5	479	201	1.88	4030	1.312	164.2	14.1	--	--
31	27.0	500	210	1.92	3833	1.307	155.6	14.2	--	--
33	31.0	639	258	1.81	4185	1.360	176.8	14.1	--	--
34	31.5	631	258	1.88	4183	1.347	175.0	14.1	--	--
14	29.7	736	298	1.88	4160	1.379	178.2	14.1	--	--
18	30.3	753	299	1.91	4077	1.379	174.6	14.2	--	--
13	30.9	738	301	1.84	4301	1.392	185.9	14.2	--	--
36	31.5	757	301	1.75	4264	1.388	183.8	14.1	--	--
35	32.0	774	308	1.84	4293	1.381	184.1	14.1	--	--
38	31.5	890	348	1.78	4444	1.413	195.0	14.1	--	--
37	31.0	889	349	1.82	4239	1.407	185.2	14.1	--	--
ϵ = 10 (Overexpanded); α = 15°; High Mixture Ratio										
9	29.5	693	302	3.31	4203	1.247	162.8	14.2	4.95	8.1
8	56.6	700	306	3.12	4548	1.251	176.7	14.1	4.97	8.0
10	31.7	705	306	3.18	4512	1.262	176.8	14.1	4.90	8.1
ϵ = 10 (Overexpanded); α = 15°; Low Mixture Ratio										
30	9.5	457	206	2.11	3536	1.197	131.4	14.2	5.26	5.7
29	8.0	486	218	2.18	3308	1.197	123.0	14.2	5.59	5.7
24	10.5	589	256	2.11	4097	1.237	157.4	14.2	5.43	6.6
17	31.0	690	299	1.69	4550	1.268	179.3	14.2	5.15	7.4
26	13.5	710	299	1.98	4085	1.275	161.8	14.1	4.88	7.6
25	11.5	712	300	2.17	3907	1.272	154.4	14.1	5.04	7.5
50	30.7	710	302	1.86	4241	1.266	166.7	14.1	5.12	7.4
39	31.2	761	326	1.78	4372	1.276	173.2	14.1	5.10	7.8
28	10.5	858	352	2.00	3859	1.308	156.7	14.2	4.78	8.2
27	14.5	883	360	1.87	4422	1.315	180.6	14.1	4.91	8.5
ϵ = 20.8 (Overexpanded); α = 15°										
75	30.4	347	167	1.72	3946	1.122	137.5	14.1	5.57	4.7
91	29.7	445	205	1.93	4196	1.174	152.9	14.1	5.62	5.3
71	30.5	575	258	--	--	1.208	--	14.1	5.16	6.5
70	30.7	706	309	1.90	4286	1.238	164.8	14.1	4.76	7.6
69	31.4	844	363	1.88	4360	1.256	170.1	14.1	4.47	9.0
89	29.8	879	374	1.84	4516	1.270	178.1	14.1	4.55	9.2
ϵ = 3.65 (Optimum); α = 10°										
88	30.7	466	189	1.80	4277	1.305	173.4	14.1	--	--
87	30.6	652	253	1.86	4176	1.366	177.3	14.1	--	--
48	30.9	768	298	1.86	4283	1.376	183.0	14.2	--	--
86	30.5	919	345	--	--	1.415	--	14.1	--	--

TABLE II (Cont'd)

Test No.	t (sec)	F (lb)	p_c (psia)	r	c^* (ft/sec)	C_F	I_{sp} (sec)	p_o (psia)	p_s (psia)	$\frac{f_s}{f_t}$
ϵ = 10 (Overexpanded); α = 10°										
54	30.6	429	195	1.86	4042	1.173	147.2	14.2	5.20	6.0
53	30.2	574	249	1.78	4091	1.239	157.4	14.2	4.98	7.1
51	30.7	703	299	1.80	4422	1.257	172.6	14.2	4.78	8.2
52	30.6	864	353	1.81	4395	1.315	179.5	14.2	4.72	9.0
ϵ = 3.65 (Optimum); α = 20°										
58	30.7	468	195	1.92	4027	1.280	160.1	14.1	--	--
57	30.8	637	254	1.87	4227	1.336	175.4	14.1	--	--
55	30.4	774	302	1.83	4415	1.364	187.0	14.1	--	--
56	30.6	899	347	1.84	4808	1.391	207.7	14.1	--	--
ϵ = 10 (Overexpanded); α = 20°										
62	30.6	434	196	1.93	4021	1.163	145.2	14.1	5.80	5.7
61	30.7	573	251	1.86	4163	1.205	155.8	14.1	5.41	6.8
60	20.2	719	302	1.93	4169	1.270	164.4	14.0	5.12	7.7
65	30.3	723	303	1.84	4337	1.260	169.7	14.1	5.32	7.65
66	31.0	850	345	1.81	4306	1.299	173.7	14.1	5.05	8.6
59	10.1	841	349	2.07	4082	1.285	162.9	14.0	4.92	8.5
ϵ = 10 (Overexpanded); α = 30°										
96	13.4	419	201	2.13	4333	1.121	150.8	14.1	5.43	5.5
95	10.8	423	204	2.07	4145	1.115	143.5	14.1	5.28	5.6
94	11.0	549	255	1.81	3845	1.158	138.3	14.1	5.32	6.45
93	10.7	688	311	1.95	4336	1.186	159.7	14.1	4.96	8.1
92	11.1	831	361	1.97	4396	1.233	168.3	14.1	4.95	9.0
Induced Separation										
40	31.2	780	330	1.85	4215	1.305	170.8	14.1	--	--
41	31.1	848	350	1.85	4255	1.327	175.3	14.1	--	--
42	27.5	850	351	1.99	4017	1.333	166.3	14.1	--	--
44	30.8	786	328	1.95	4054	1.334	167.9	14.1	--	--
45	30.1	584	255	1.99	3964	1.259	155.0	14.1	--	--
47	61.7	729	308	1.87	4323	1.300	174.5	14.2	--	--

Figure 1
Underexpansion of Rocket Motor Flame

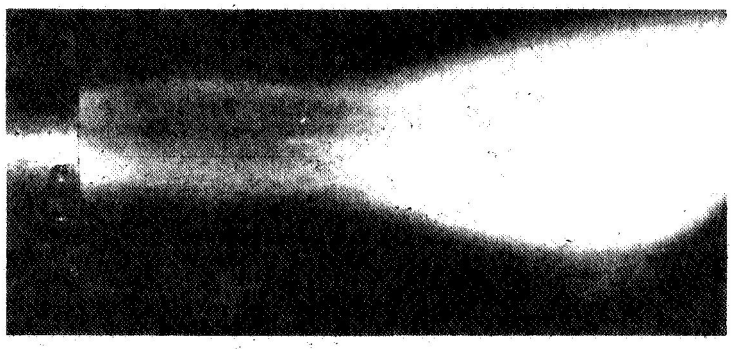

Figure 2
Correct Expansion of Rocket Motor Flame

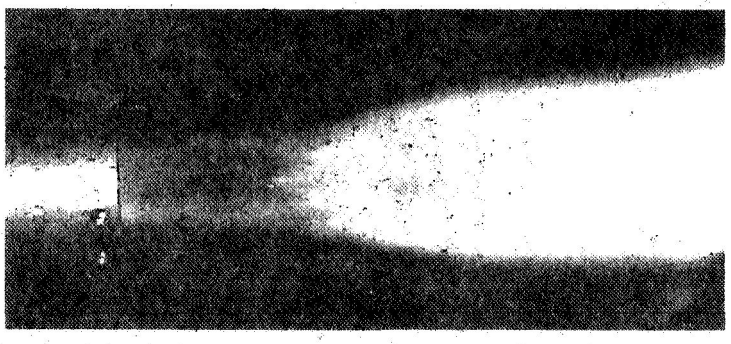

Figure 3
Overexpansion of Rocket Motor Flame Without Jet Separation

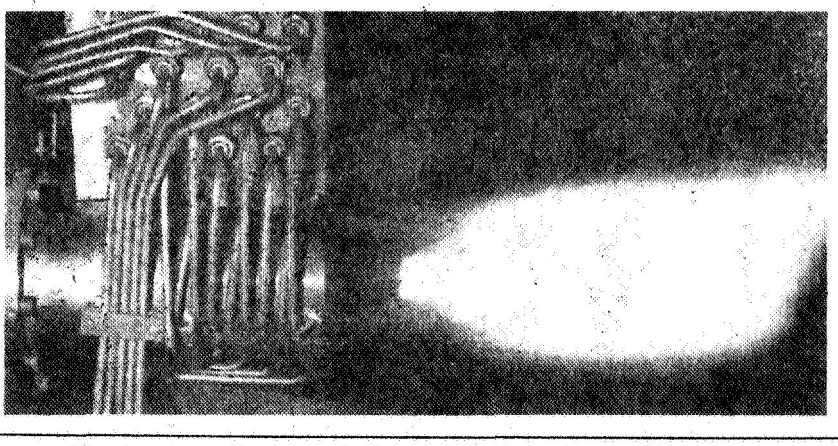

Figure 4. Overexpansion of Rocket Motor Flame With Jet Separation

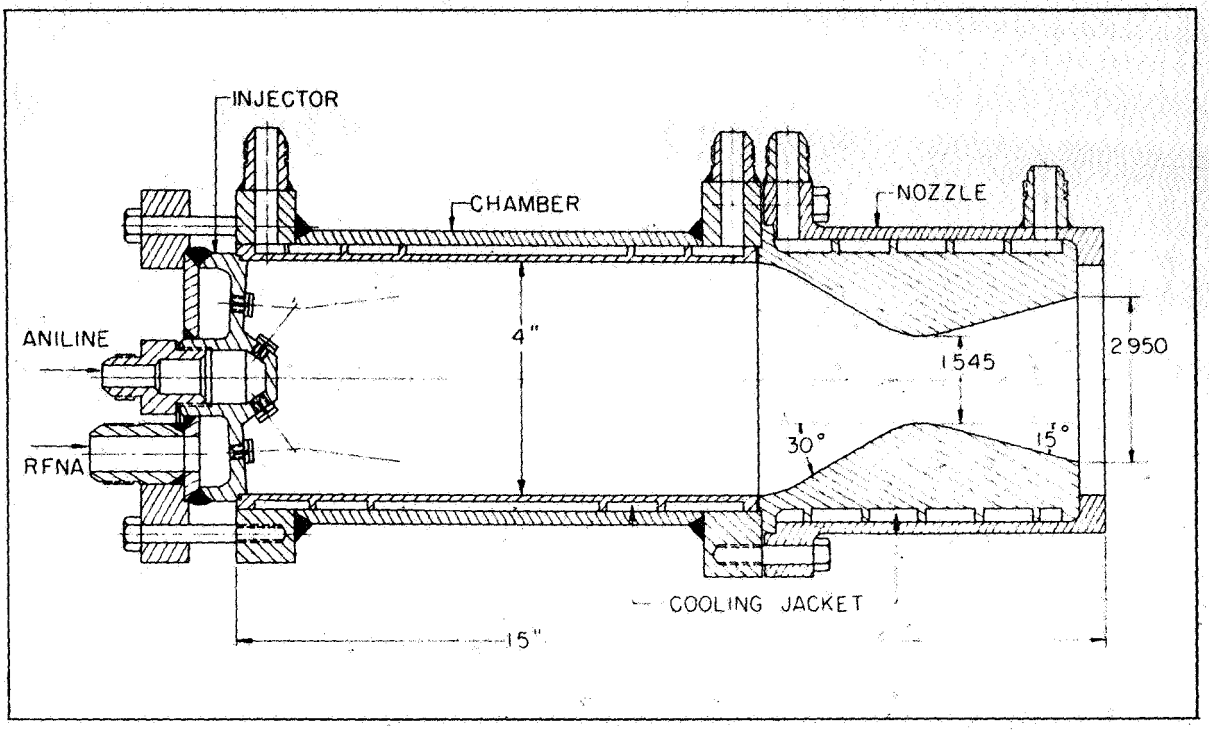

Figure 5. Test Rocket Motor with Optimum Expansion Nozzle

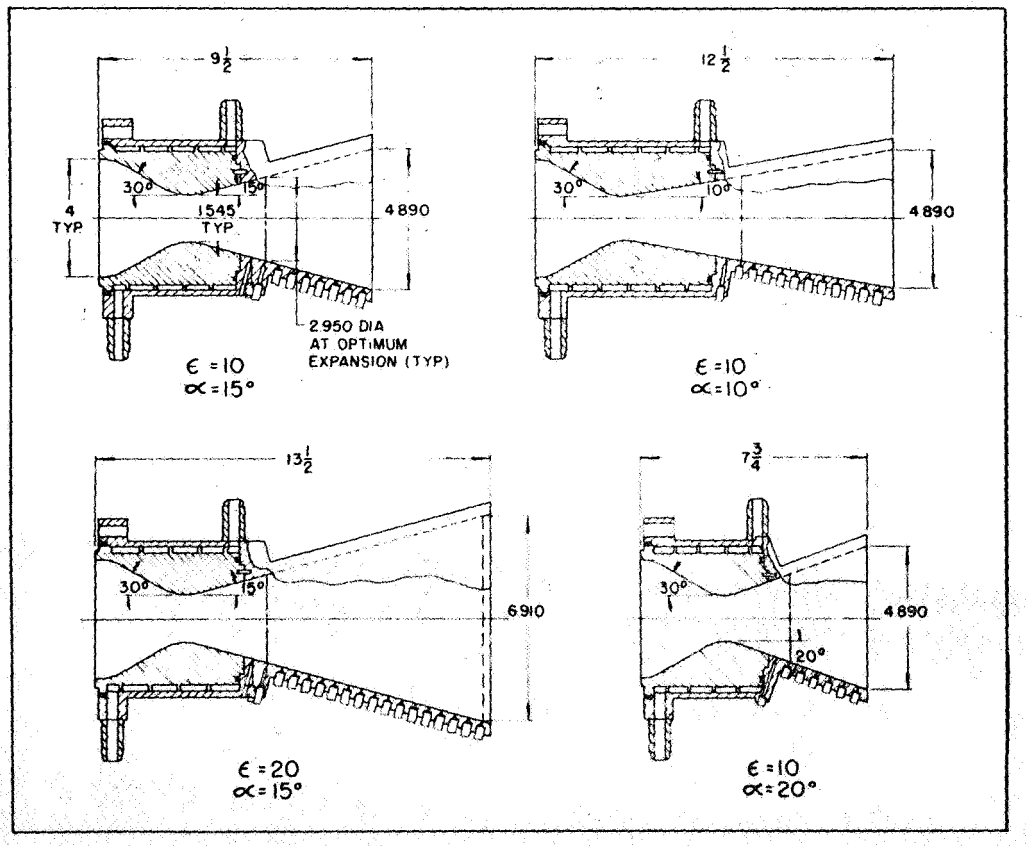

Figure 6. Overexpanded Nozzles

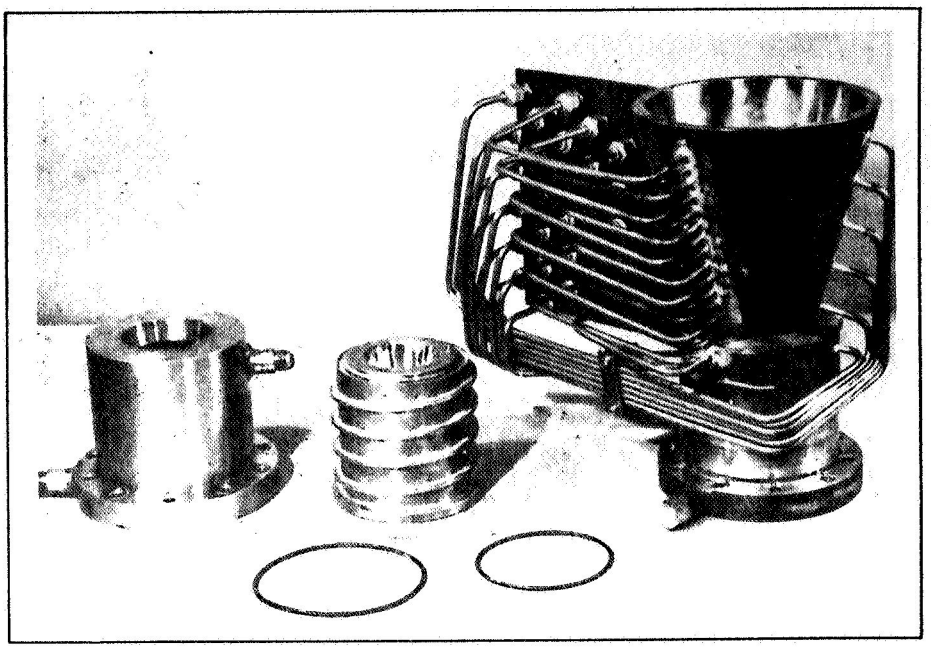

Figure 7. Typical Test Nozzle

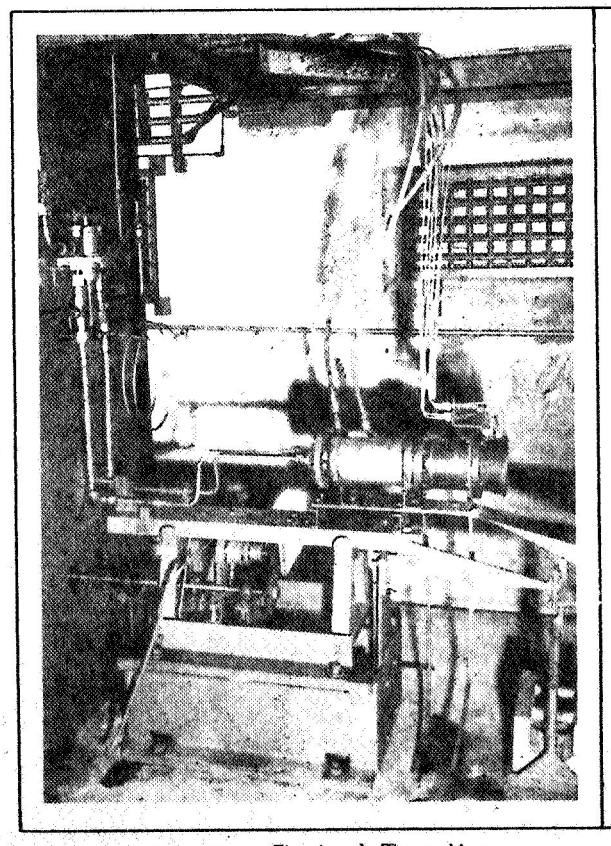

Figure 8. Typical Test Motor Installation

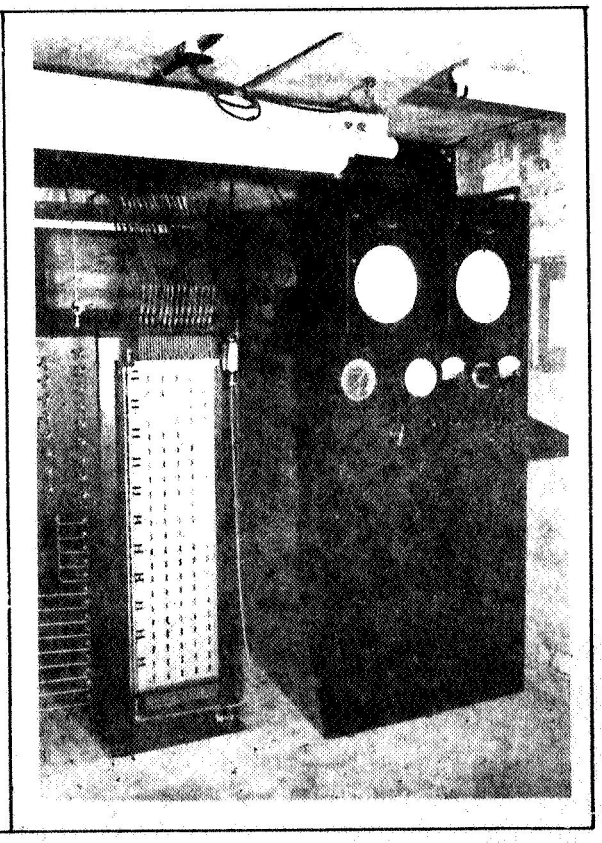

Figure 9. Control Panel and Manometer Bank

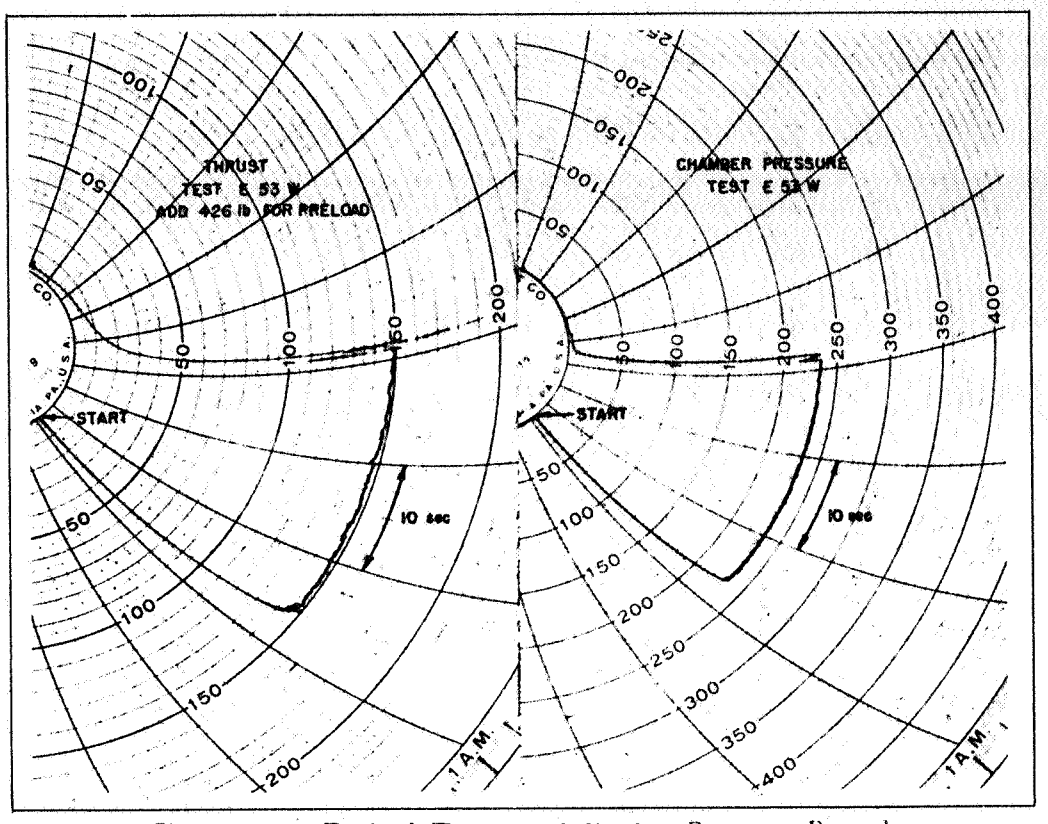

Figure 10. Typical Thrust and Chamber Pressure Records

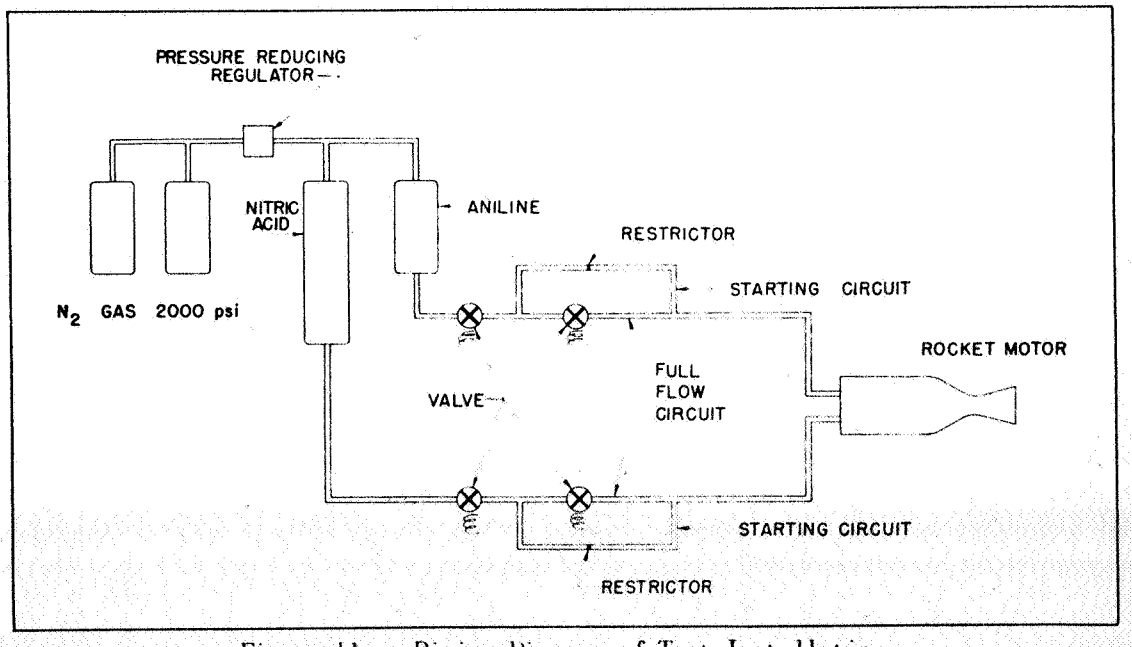

Figure 11. Piping Diagram of Test Installation

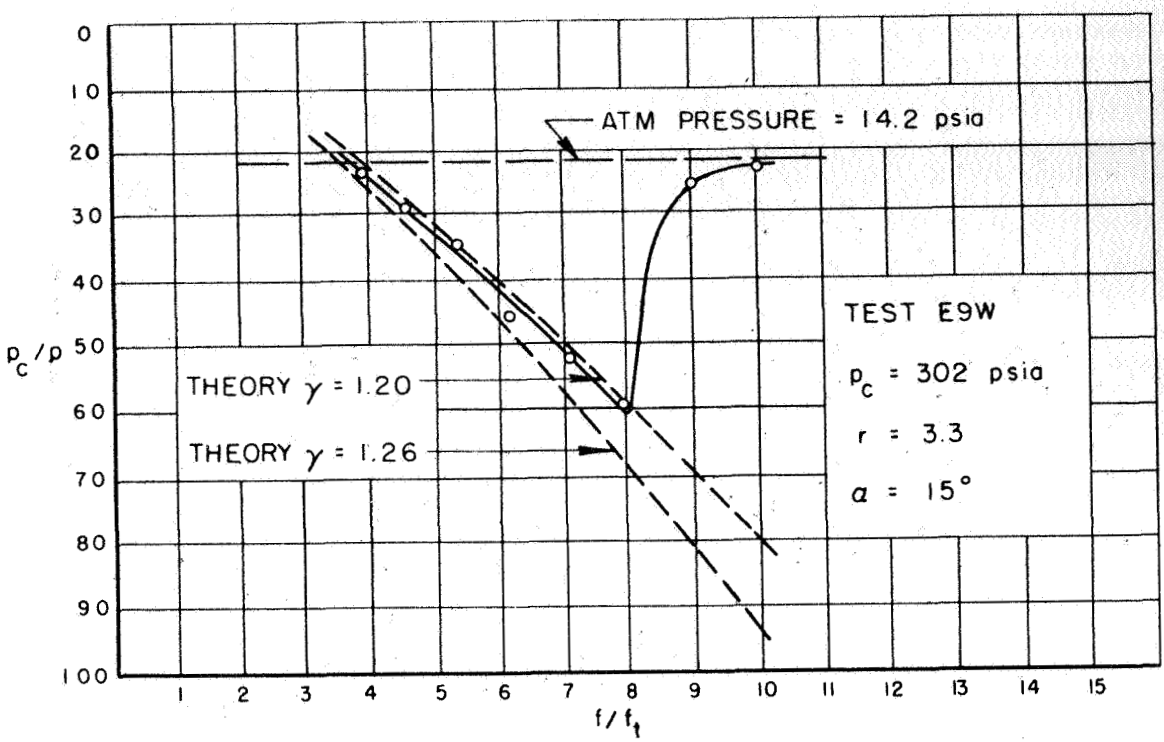

Figure 12. Pressure in Overexpanded Nozzle, ϵ = 10, α = 15°, High Mixture Ratio

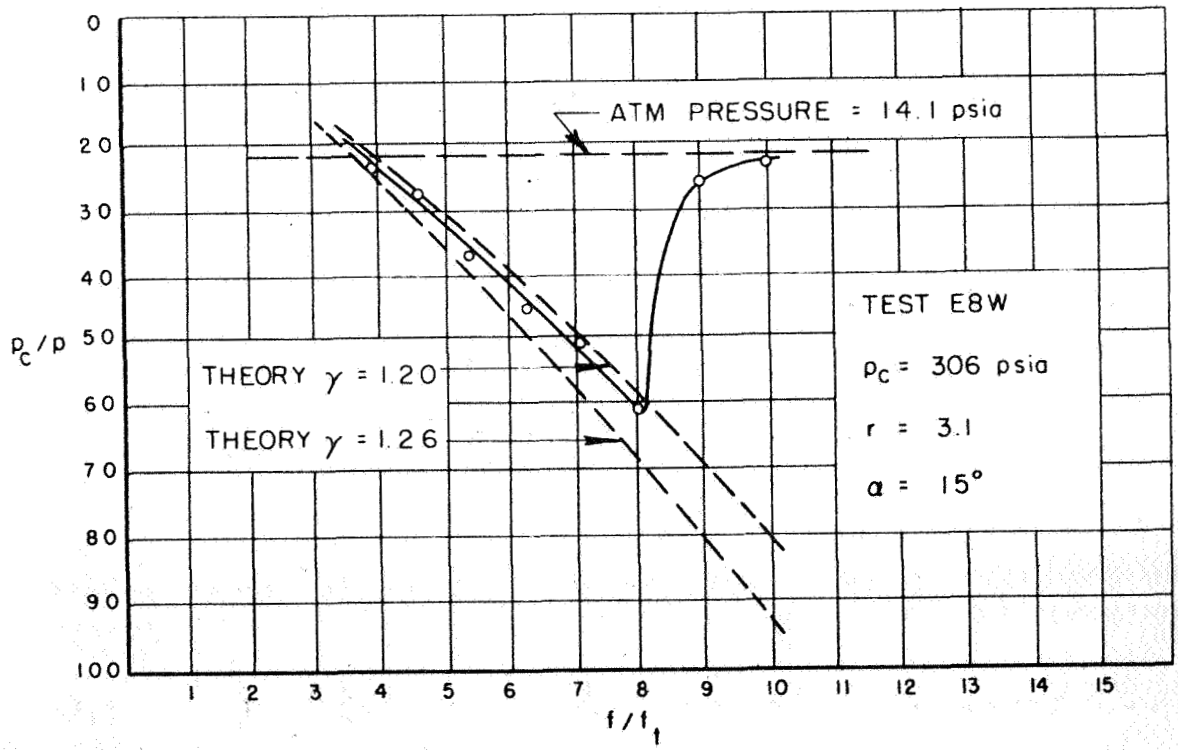

Figure 13. Pressure in Overexpanded Nozzle, ϵ = 10, α = 15°, High Mixture Ratio

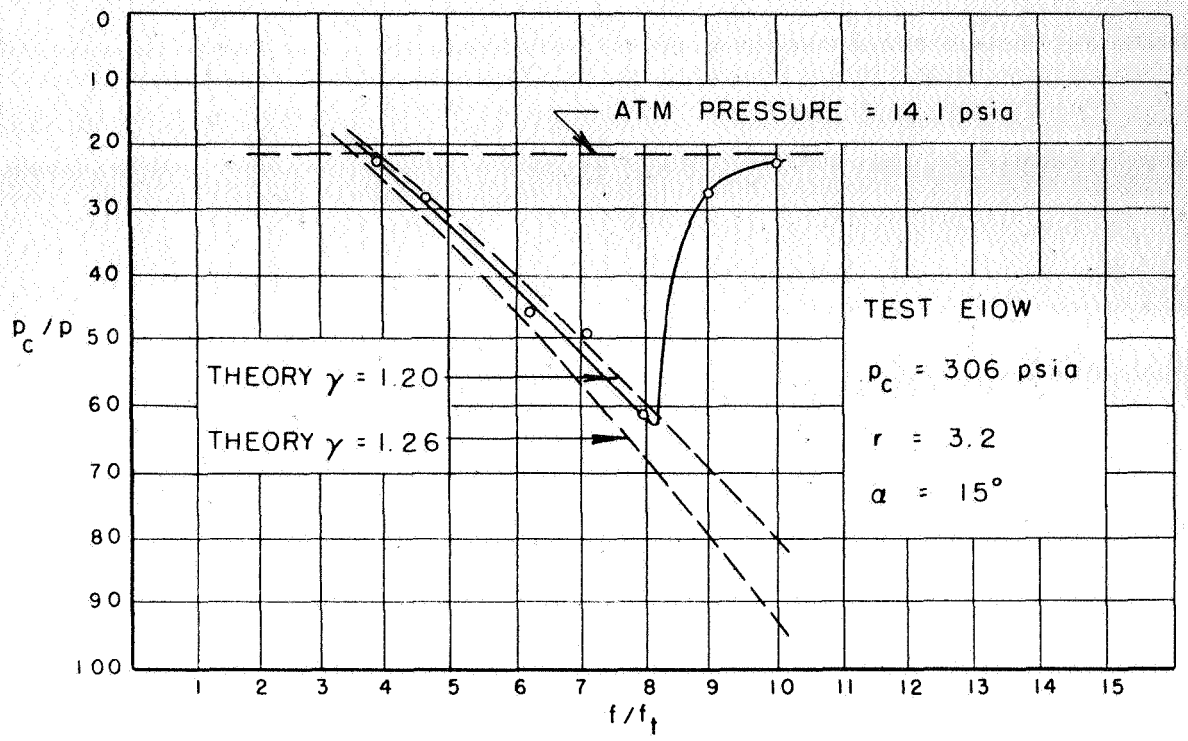

Figure 14. Pressure in Overexpanded Nozzle, ϵ = 10, α = 15°, High Mixture Ratio

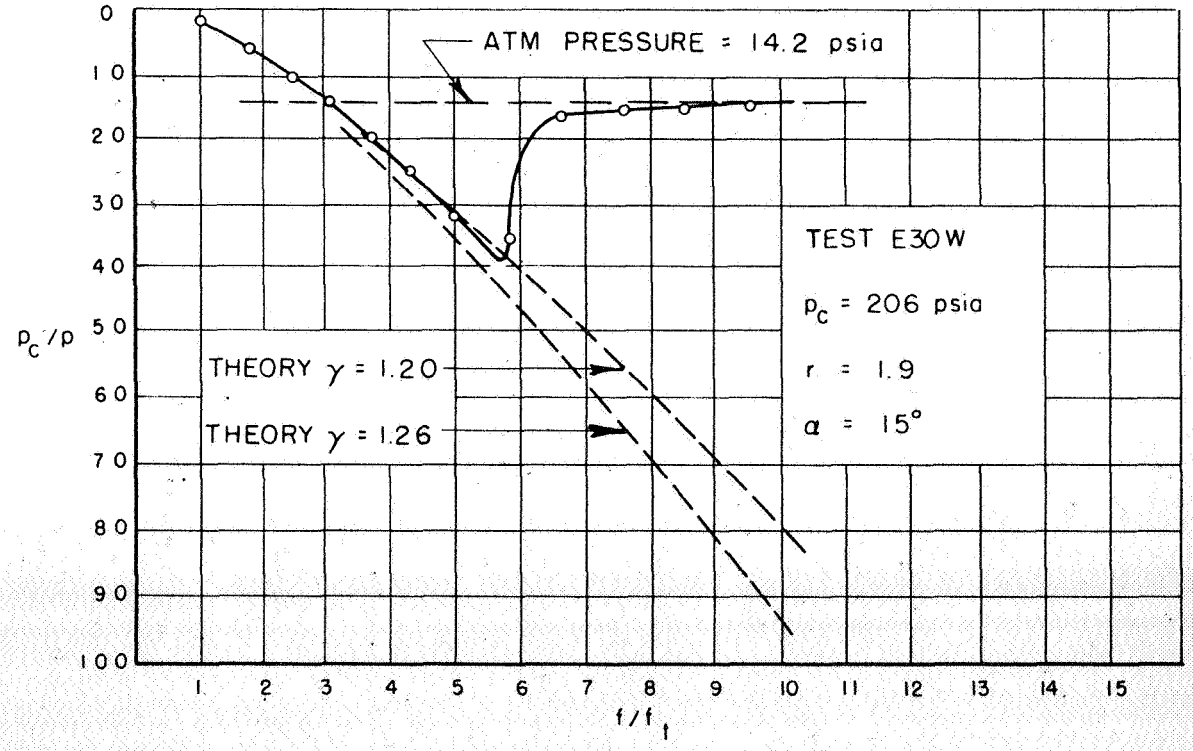

Figure 15. Pressure in Overexpanded Nozzle, ϵ = 10, α = 15°, $p_c \cong$ 200 psia

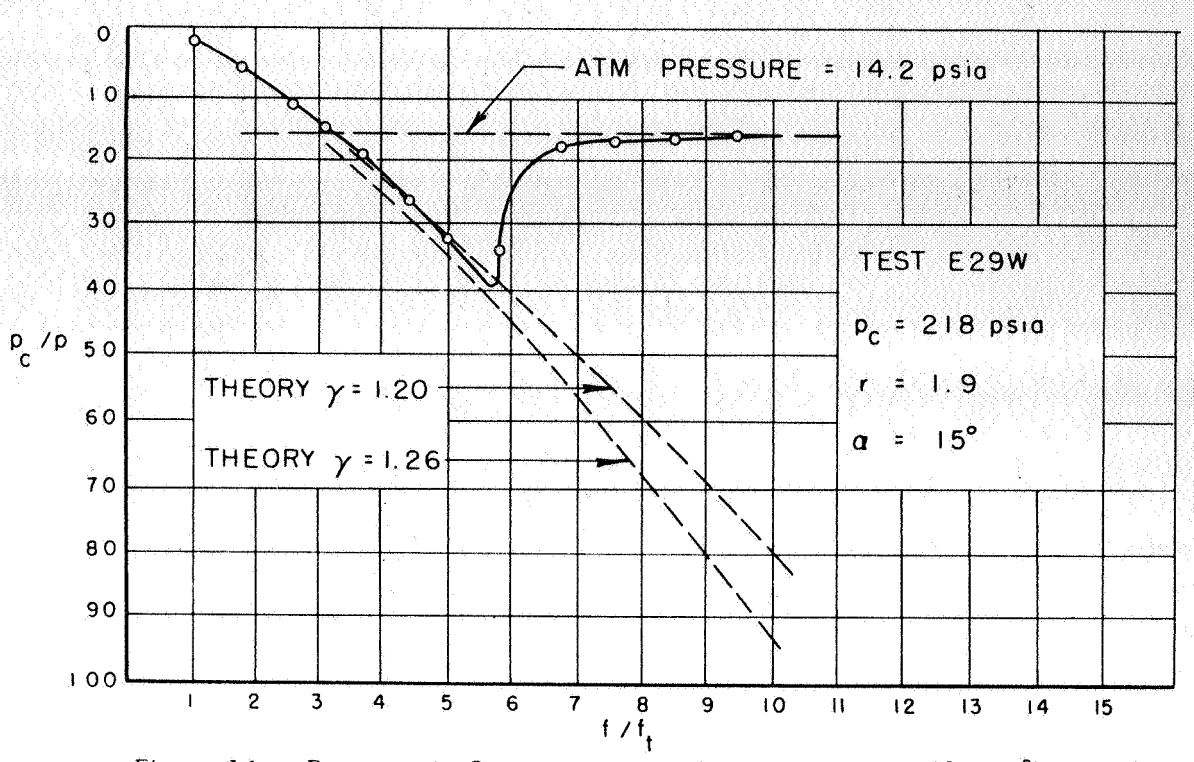

Figure 16. Pressure in Overexpanded Nozzle, $\epsilon = 10$, $\alpha = 15°$, $p_c \cong 200$ psia

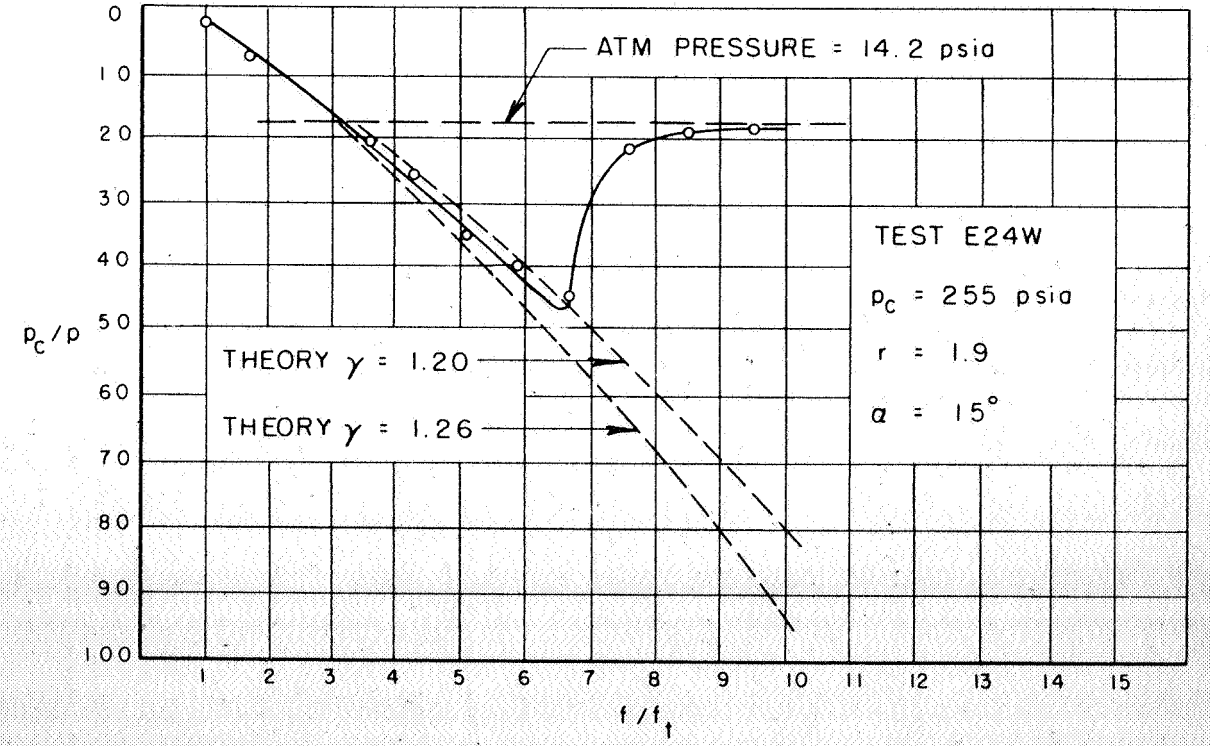

Figure 17. Pressure in Overexpanded Nozzle, $\epsilon = 10$, $\alpha = 15°$, $p_c \cong 250$ psia

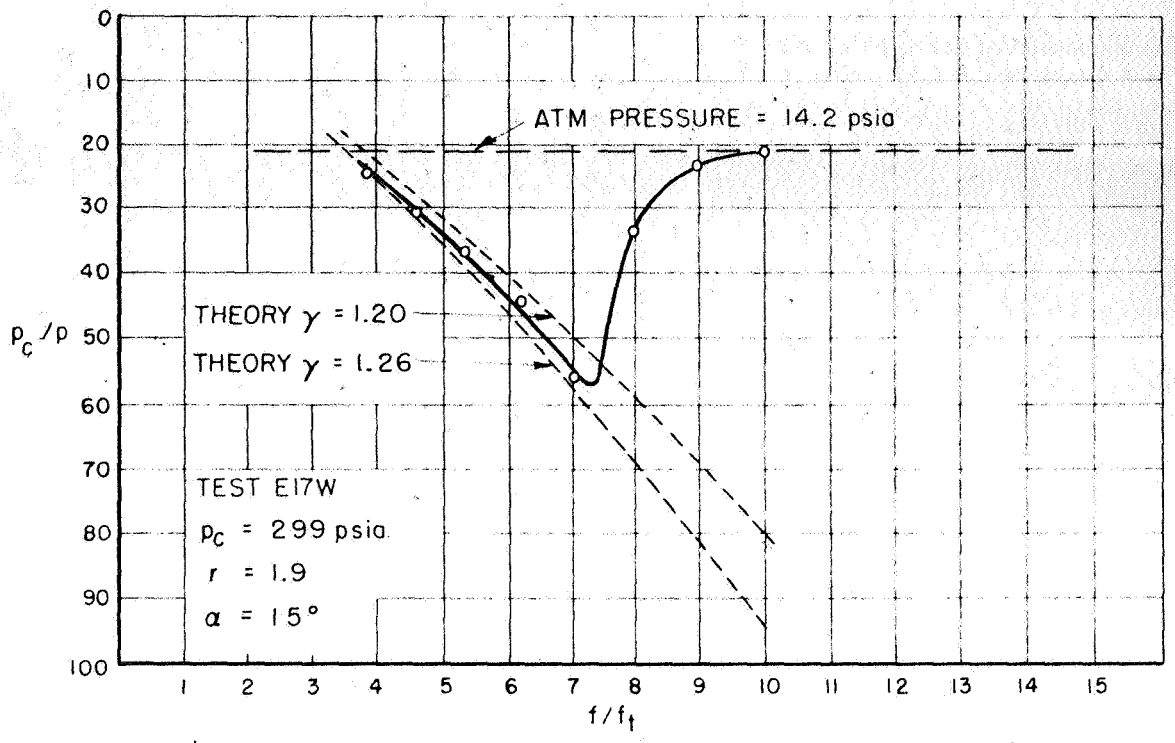

Figure 18. Pressure in Overexpanded Nozzle, $\epsilon = 10$, $\alpha = 15°$, $p_c \cong 300$ psia

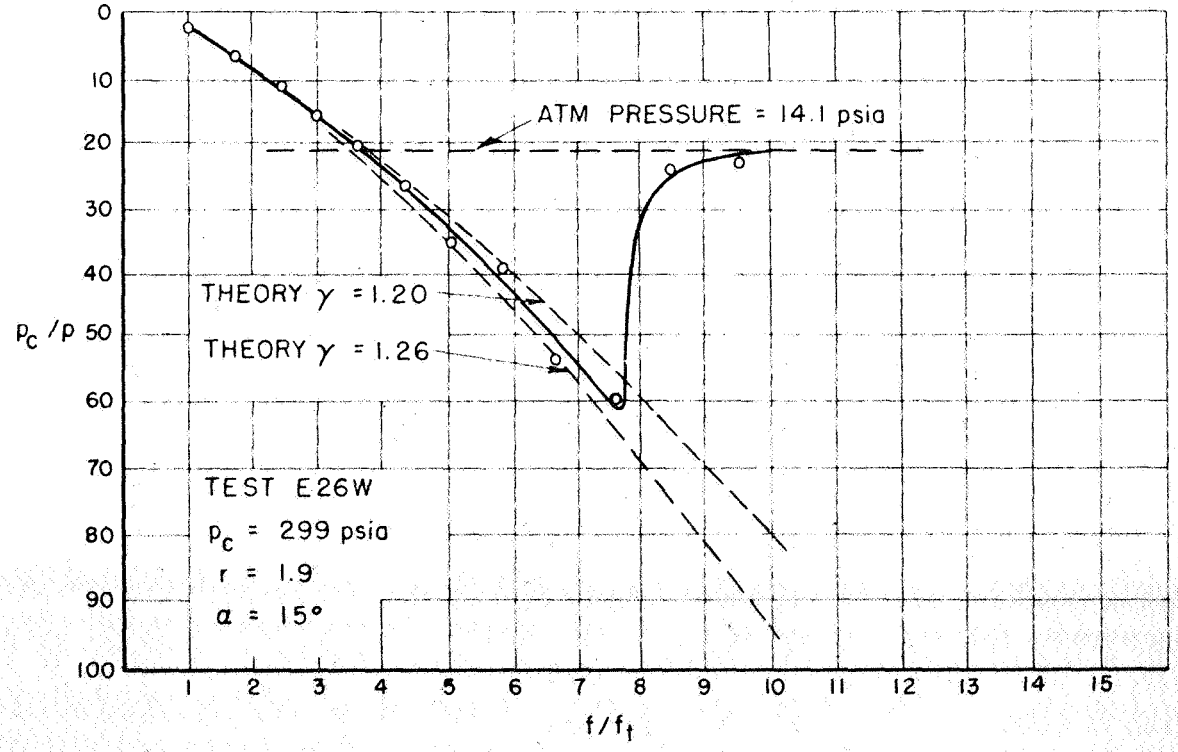

Figure 19. Pressure in Overexpanded Nozzle, $\epsilon = 10$, $\alpha = 15°$, $p_c \cong 300$ psia

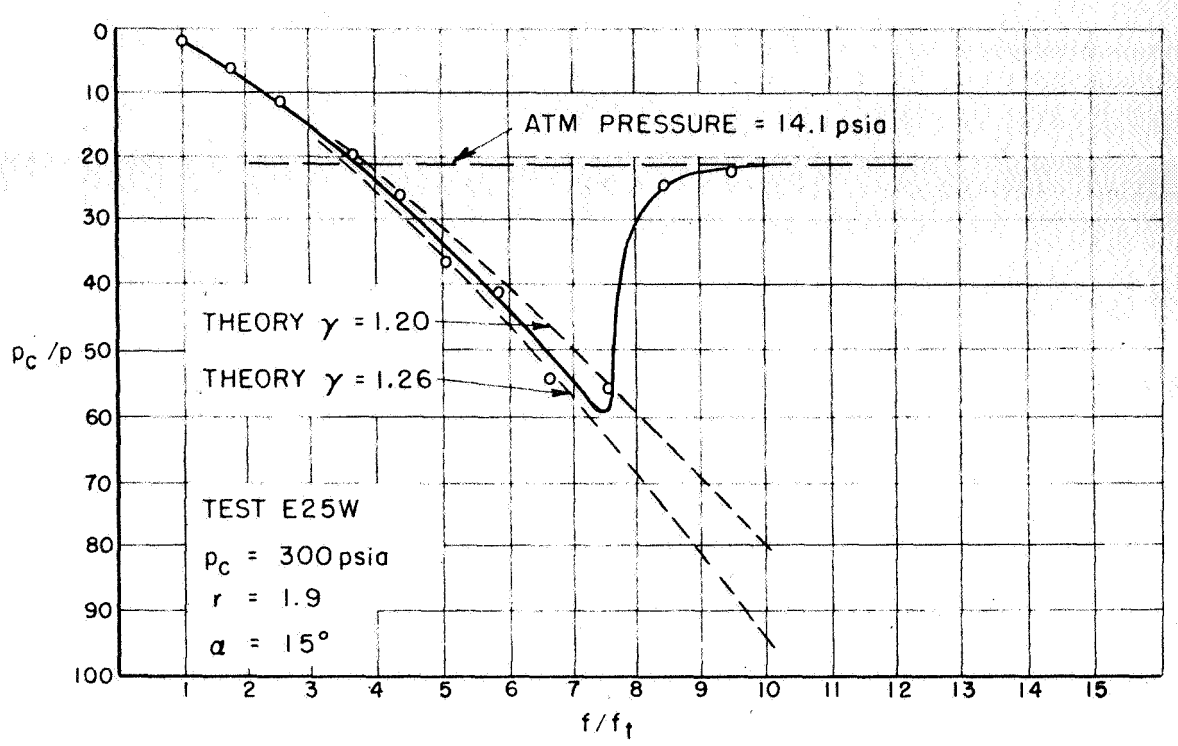

Figure 20. Pressure in Overexpanded Nozzle, ϵ = 10, α = 15°, $p_c \cong$ 300 psia

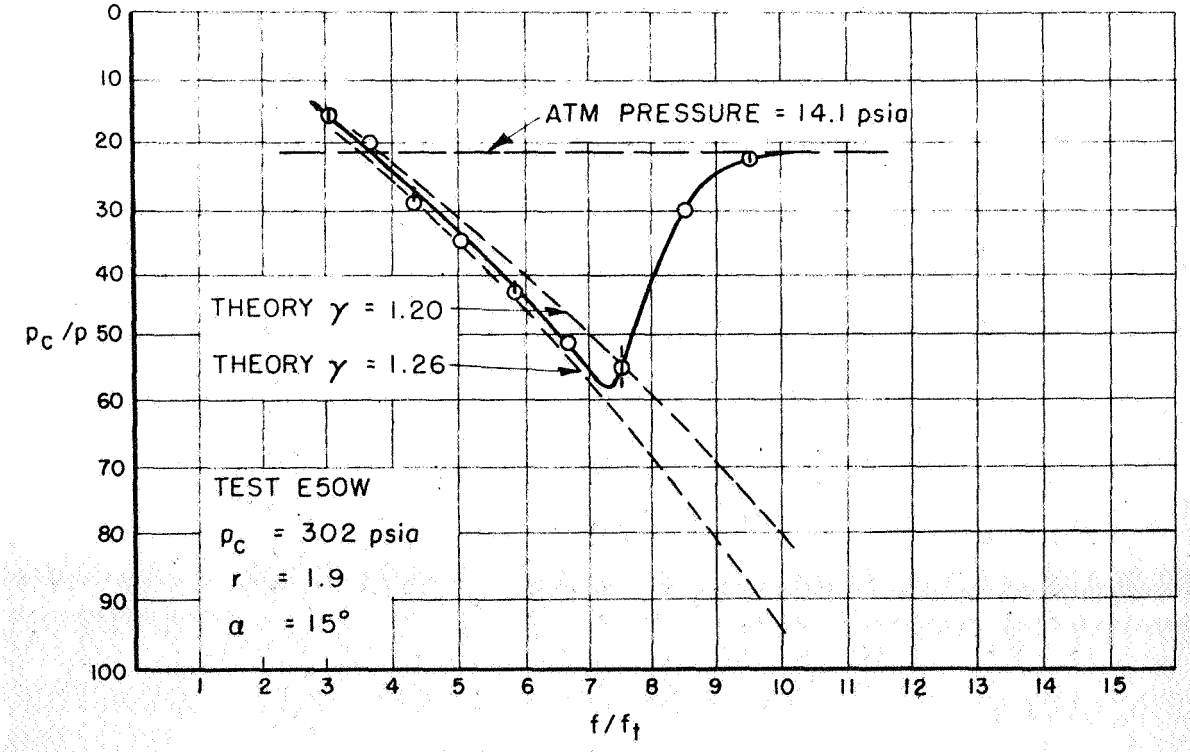

Figure 21. Pressure in Overexpanded Nozzle, ϵ = 10, α = 15°, $p_c \cong$ 300 psia

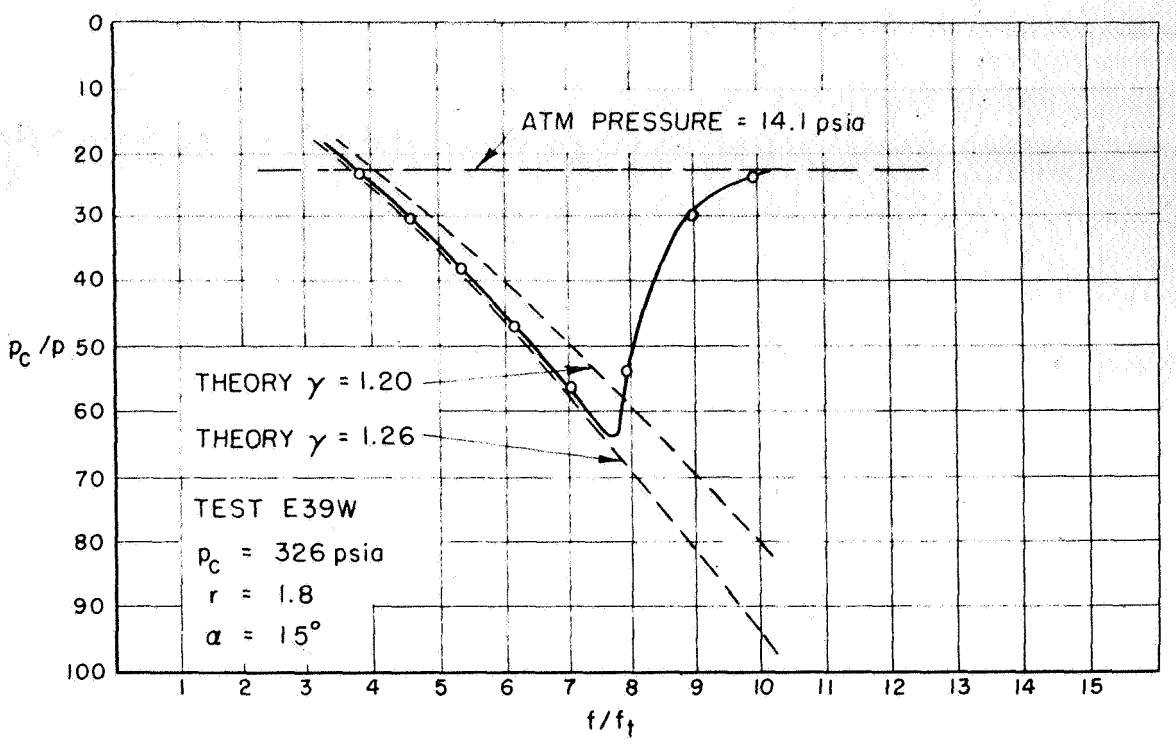

Figure 22. Pressure in Overexpanded Nozzle, $\epsilon = 10$, $\alpha = 15°$, $p_c \cong 330$ psia

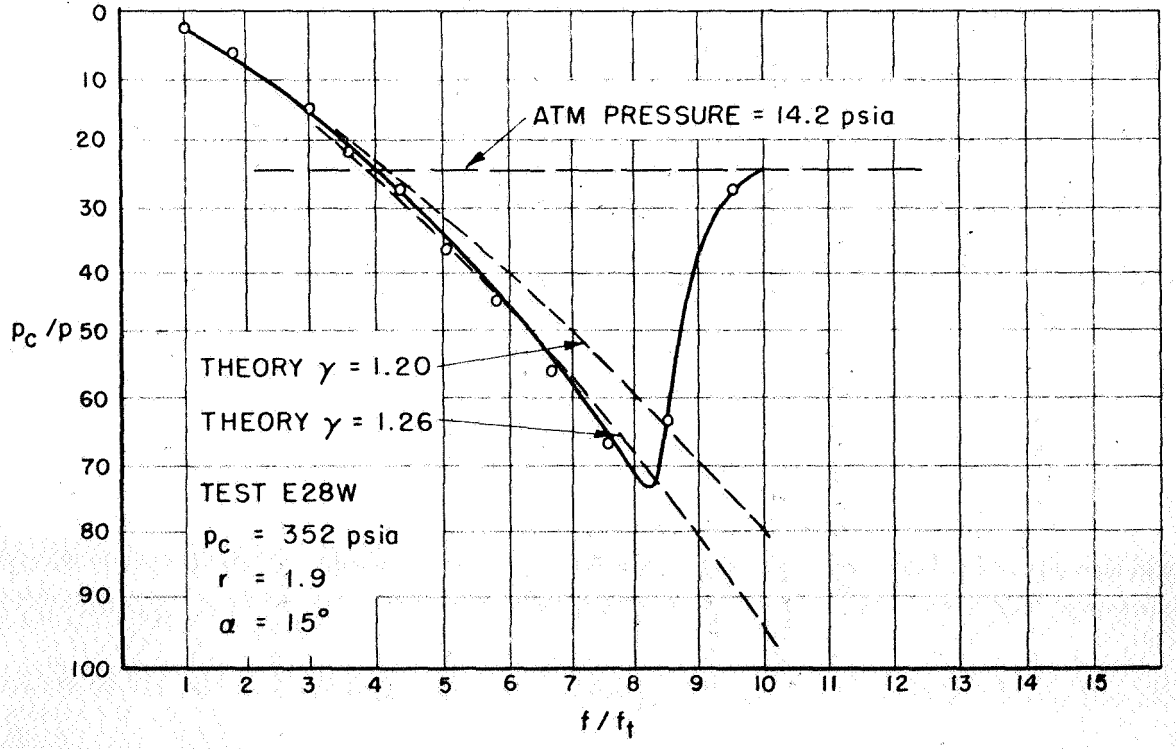

Figure 23. Pressure in Overexpanded Nozzle, $\epsilon = 10$, $\alpha = 15°$, $p_c \cong 350$ psia

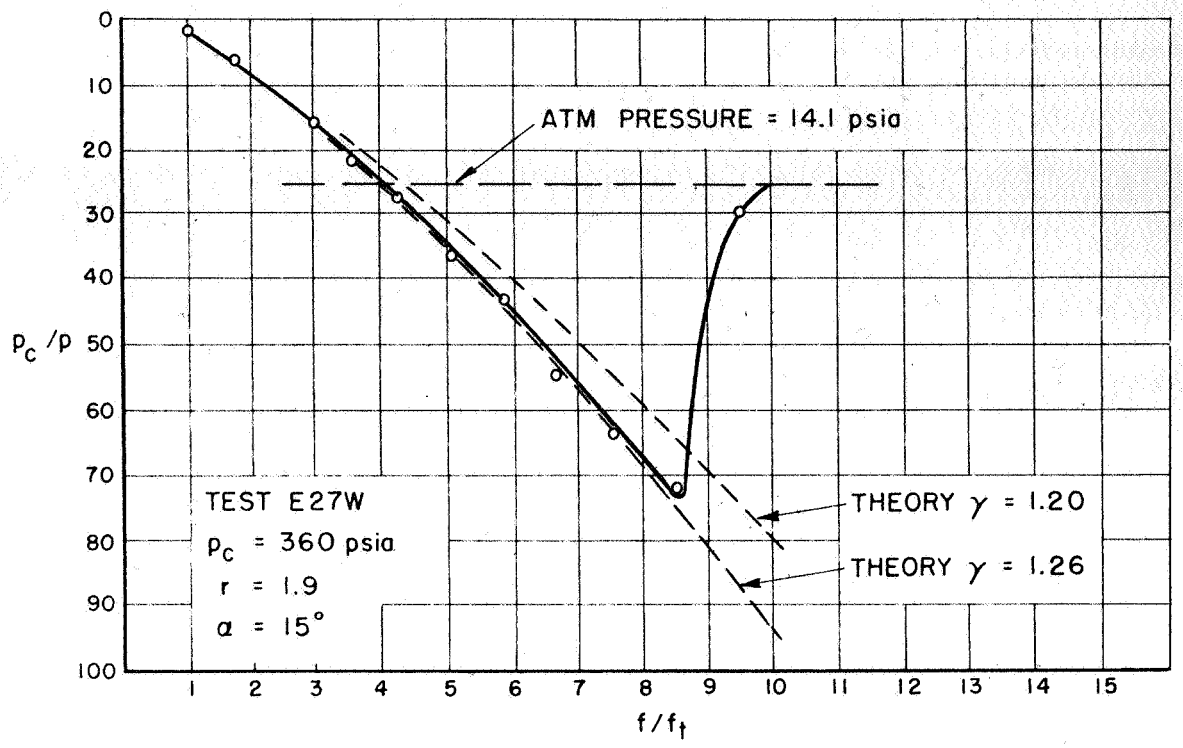

Figure 24. Pressure in Overexpanded Nozzle, $\epsilon = 10$, $\alpha = 15°$, $p_c \tilde{=} 350$ psia

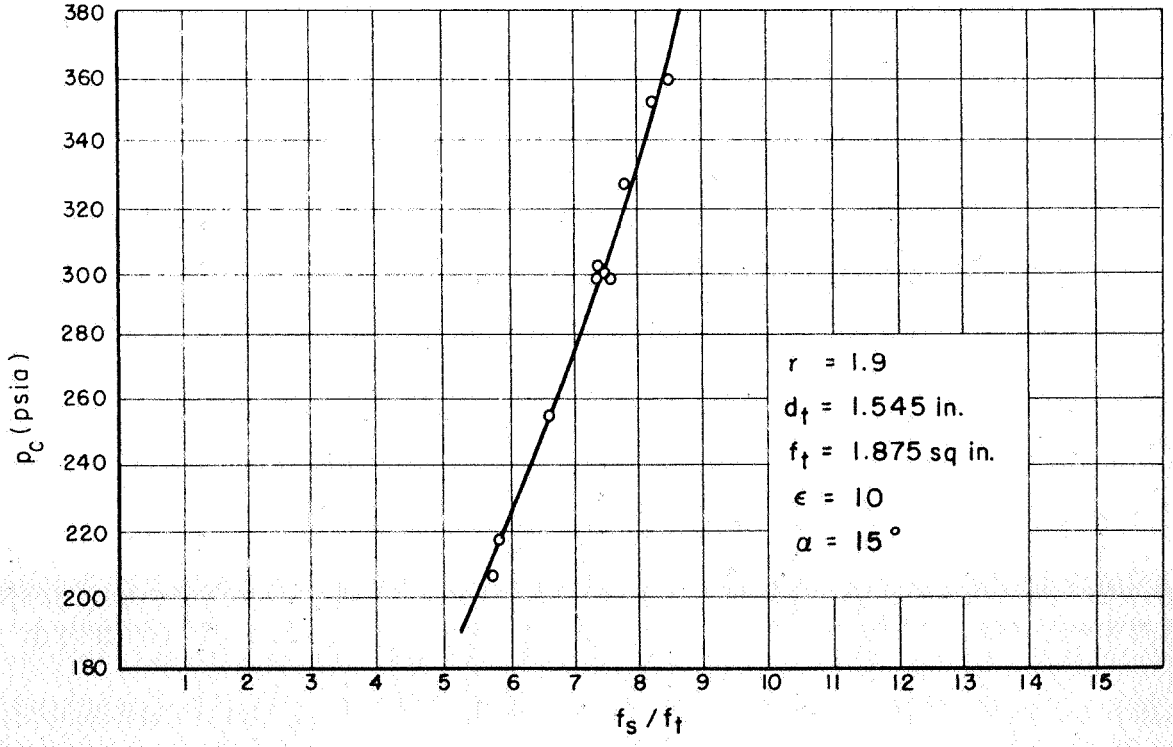

Figure 25. Area Ratio at Plane of Separation vs Chamber Pressure for $\epsilon = 10$, $\alpha = 15°$

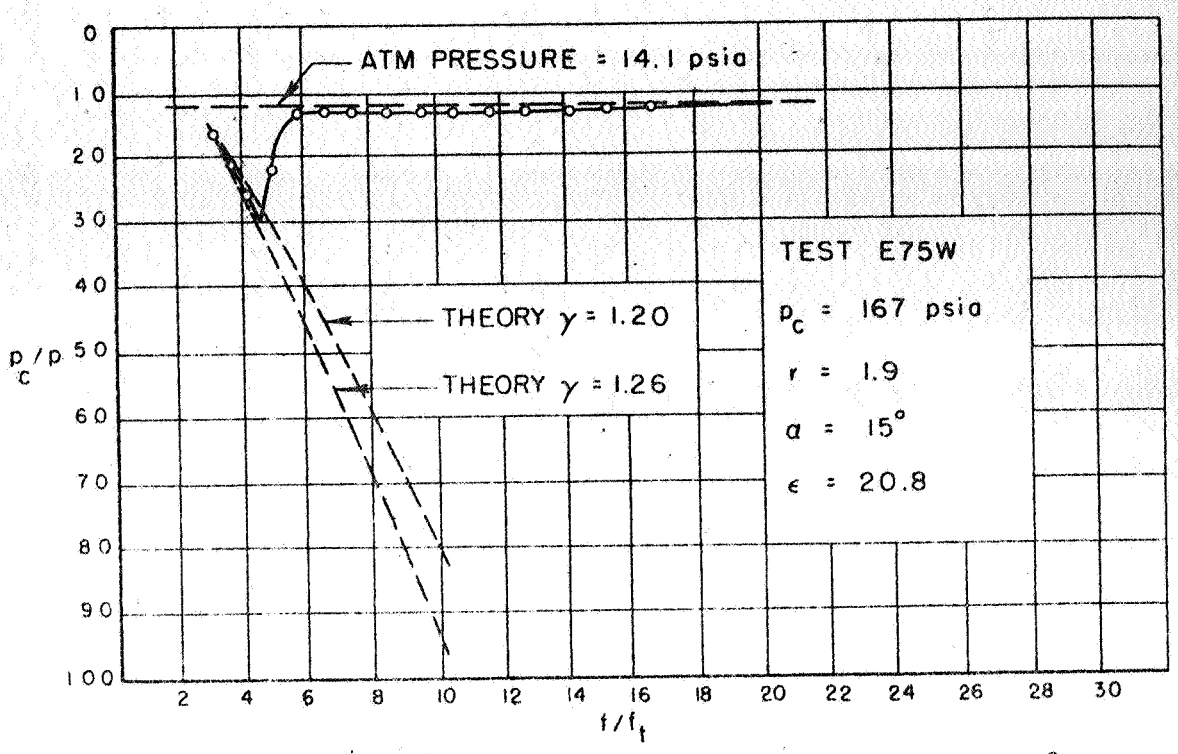

Figure 26. Pressure in Overexpanded Nozzle, $\epsilon = 20.8$, $\alpha = 15°$

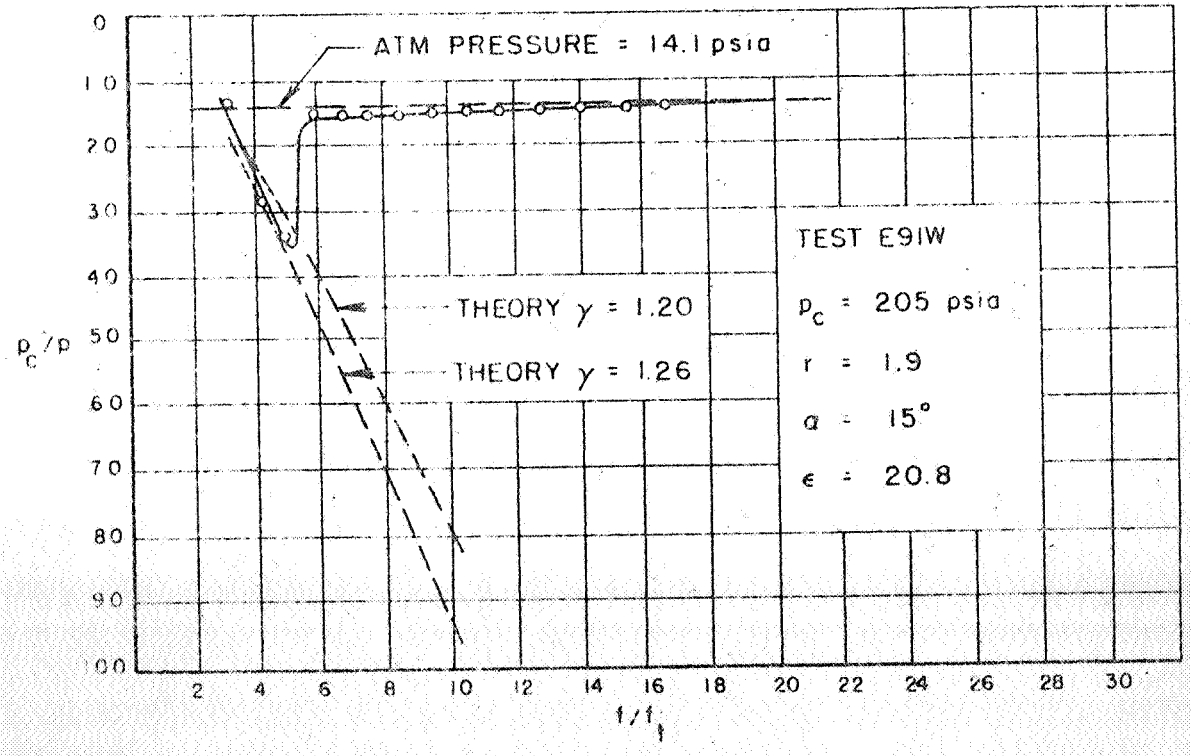

Figure 27. Pressure in Overexpanded Nozzle, $\epsilon = 20.8$, $\alpha = 15°$

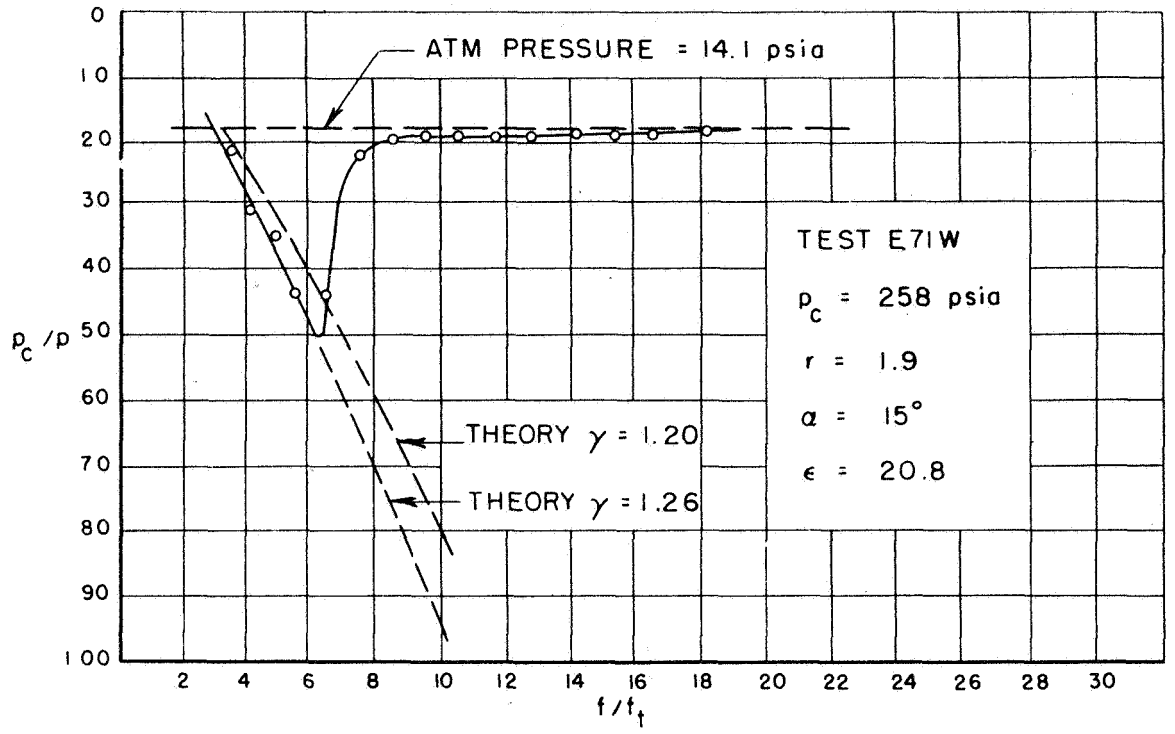

Figure 28. Pressure in Overexpanded Nozzle, $\epsilon = 20.8$, $\alpha = 15°$

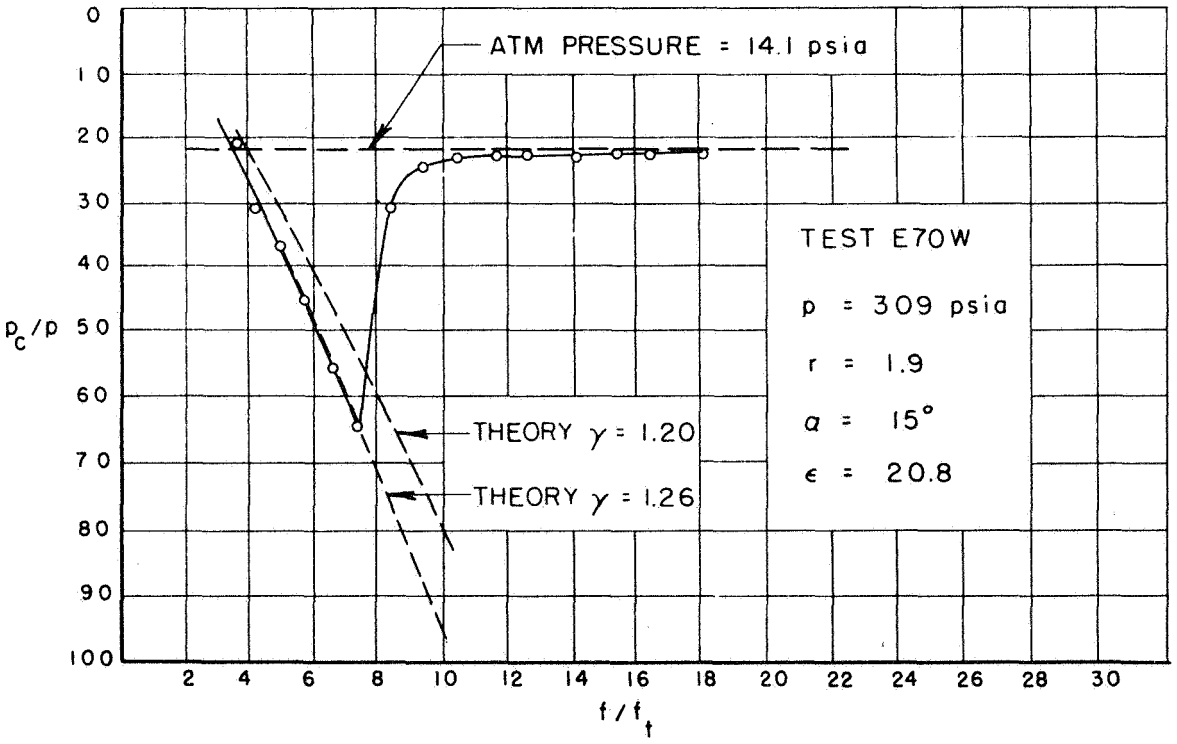

Figure 29. Pressure in Overexpanded Nozzle, $\epsilon = 20.8$, $\alpha = 15°$

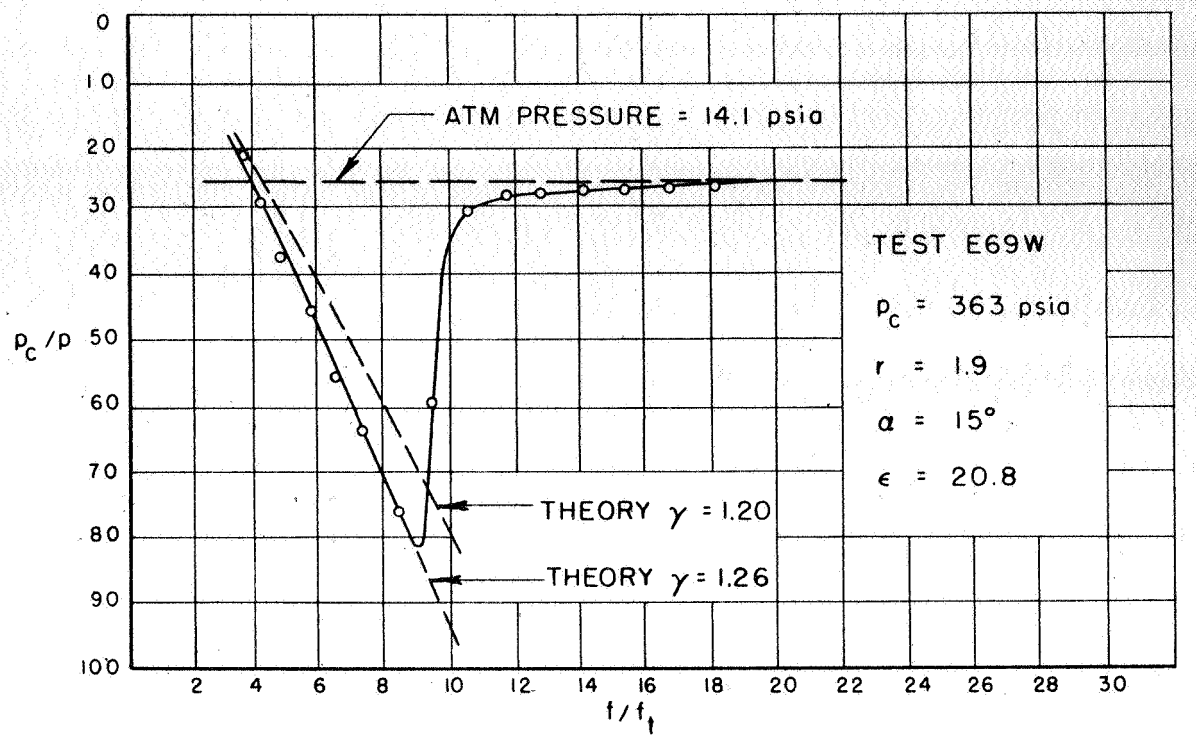

Figure 30. Pressure in Overexpanded Nozzle, $\epsilon = 20.8$, $\alpha = 15°$

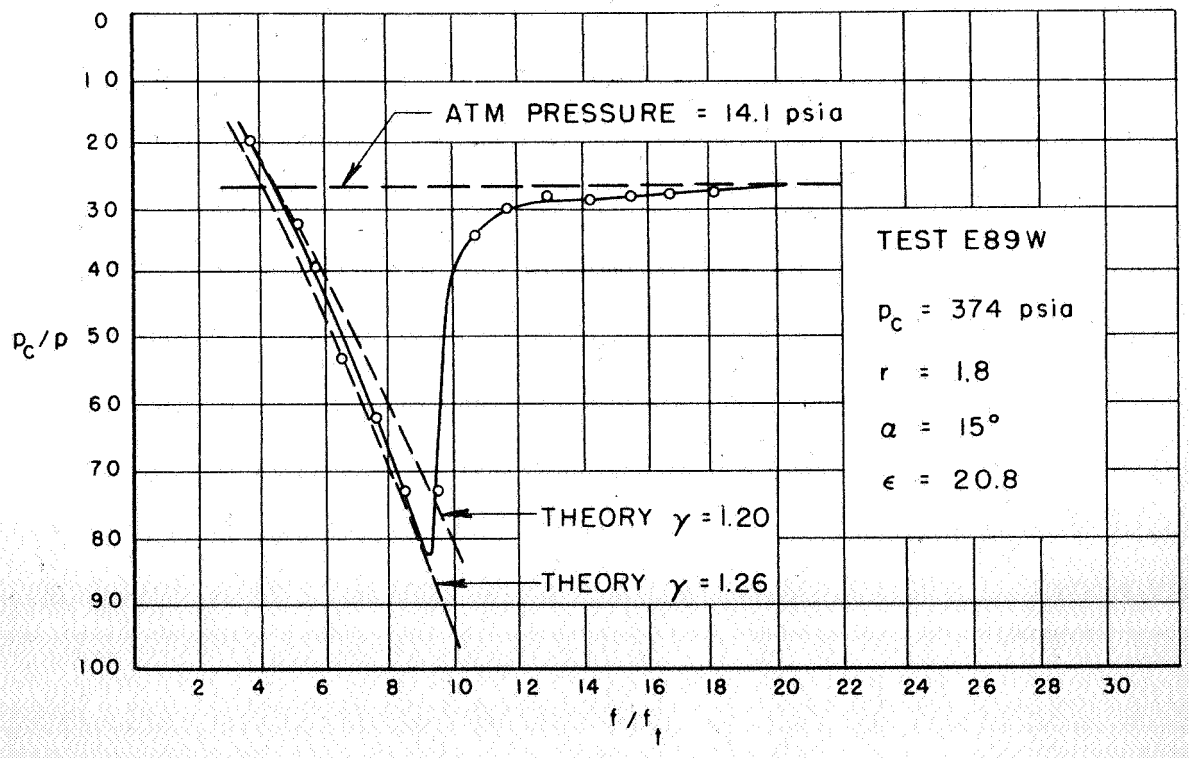

Figure 31. Pressure in Overexpanded Nozzle, $\epsilon = 20.8$, $\alpha = 15°$

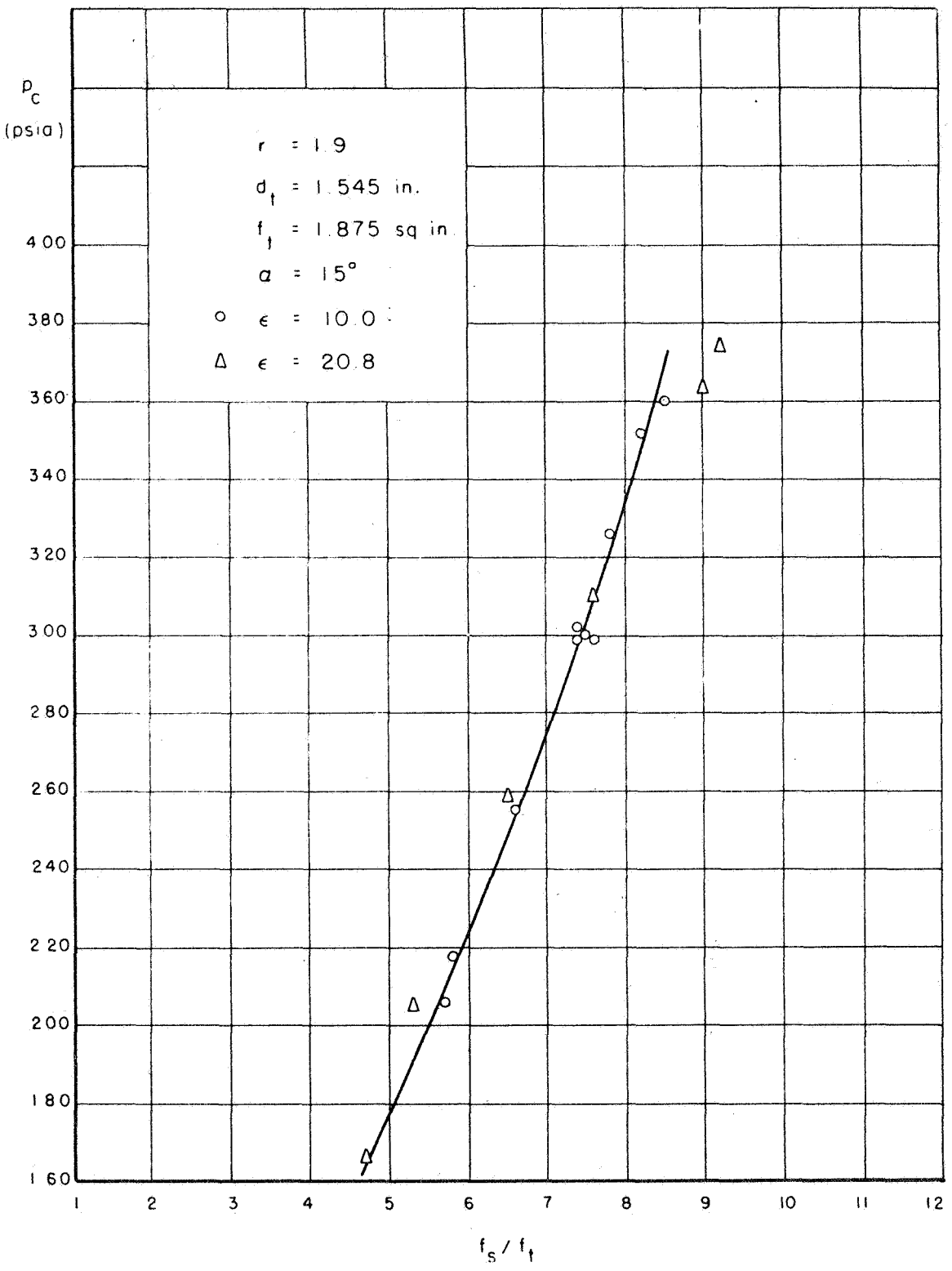

Figure 32. Area Ratio at Plane of Separation vs Chamber Pressure for $\alpha = 15°$, $\epsilon = 10.0$ and 20.8

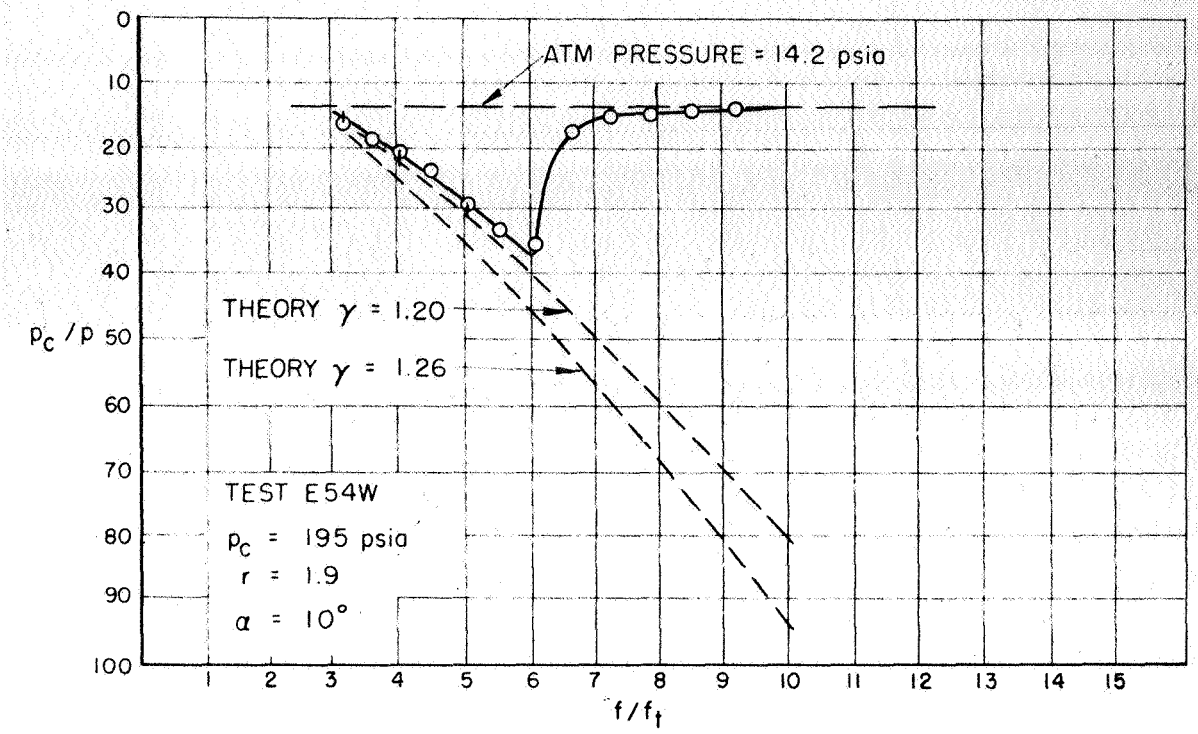

Figure 33. Pressure in Overexpanded Nozzle, ϵ = 10.0, α = 10°

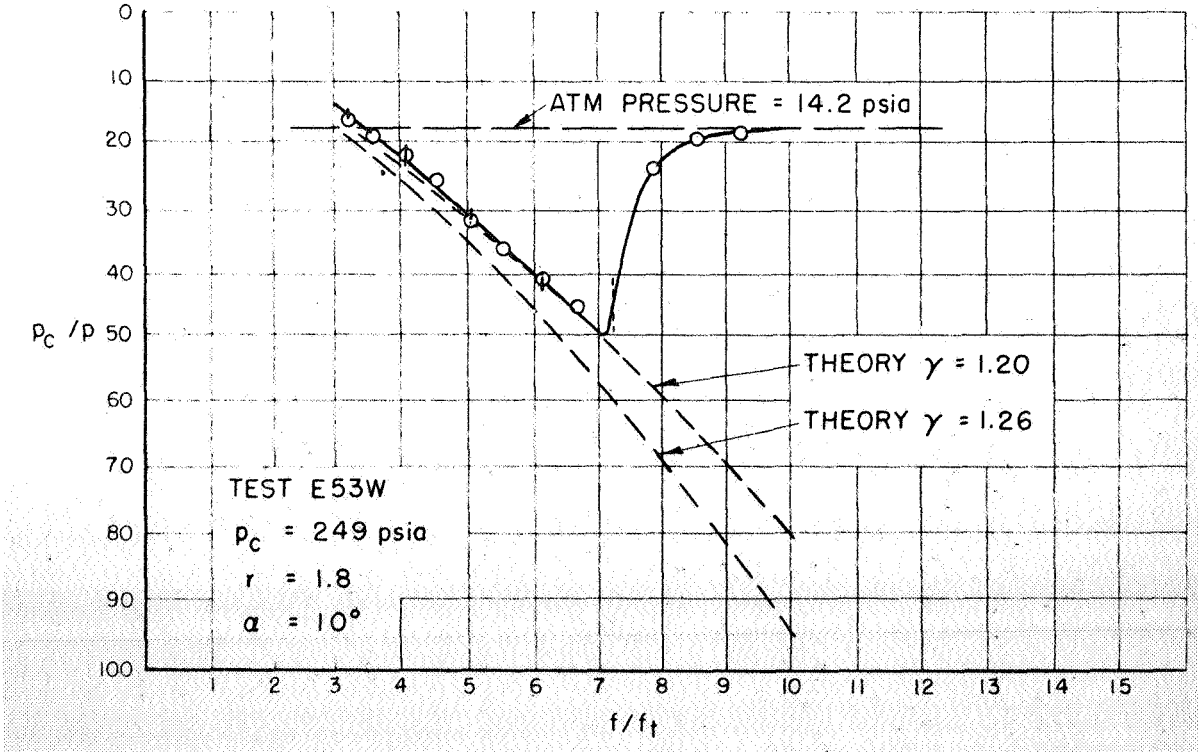

Figure 34. Pressure in Overexpanded Nozzle, ϵ = 10.0, α = 10°

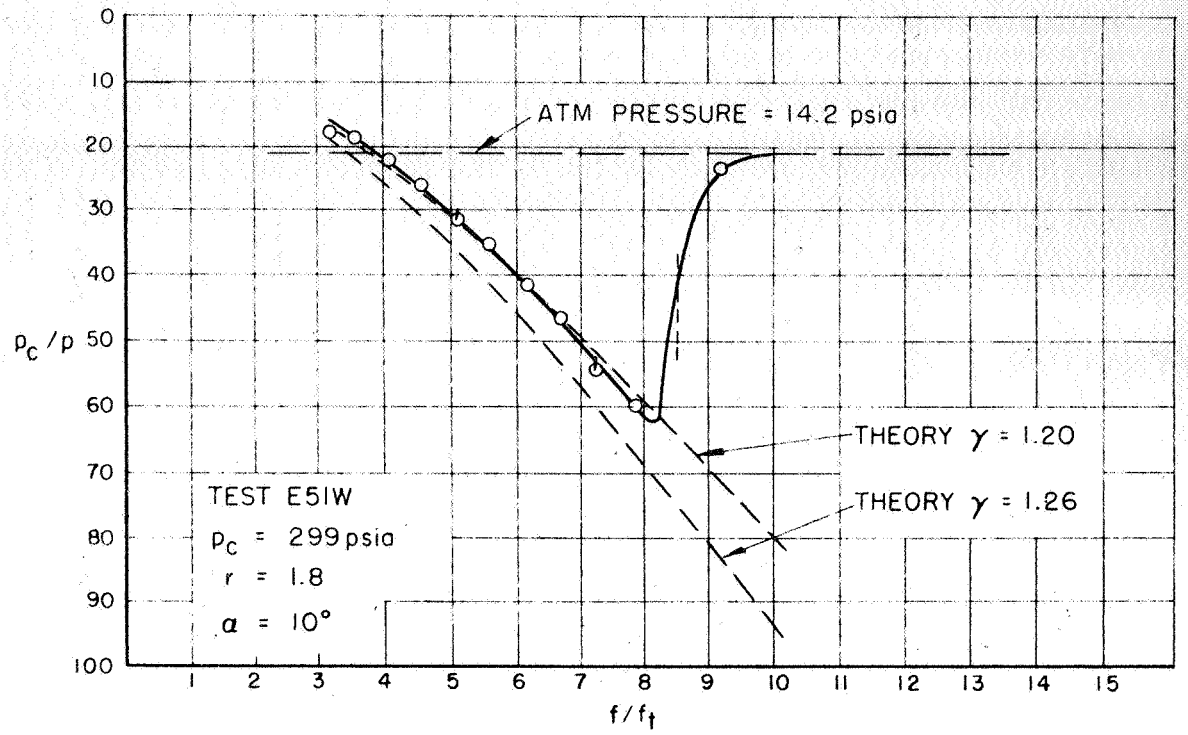

Figure 35. Pressure in Overexpanded Nozzle, ϵ = 10.0, α = 10°

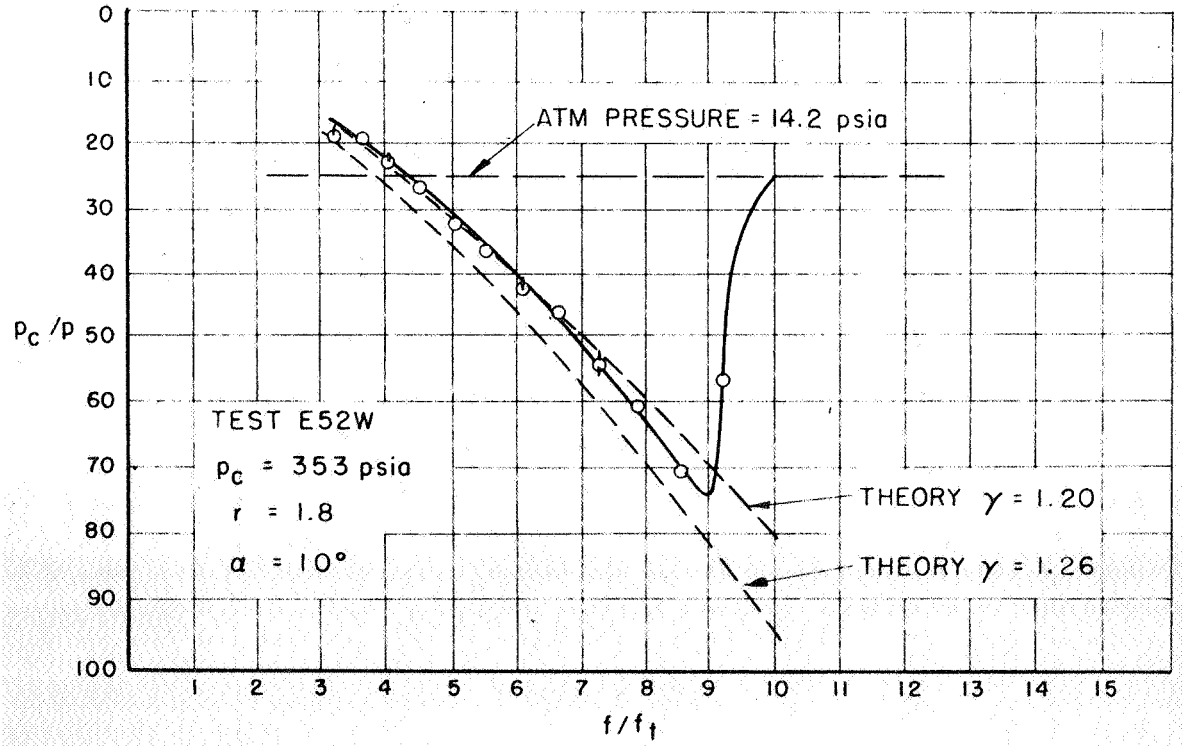

Figure 36. Pressure in Overexpanded Nozzle, ϵ = 10.0, α = 10°

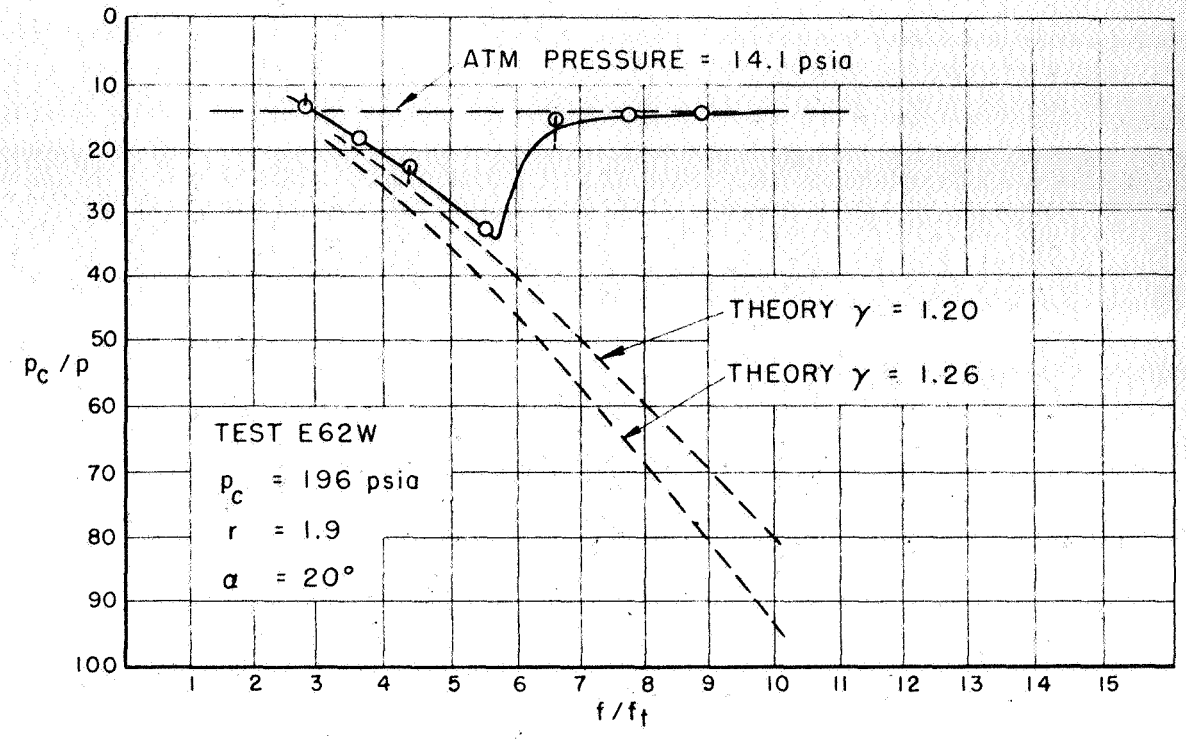

Figure 37. Pressure in Overexpanded Nozzle, ϵ = 10.0, α = 20°

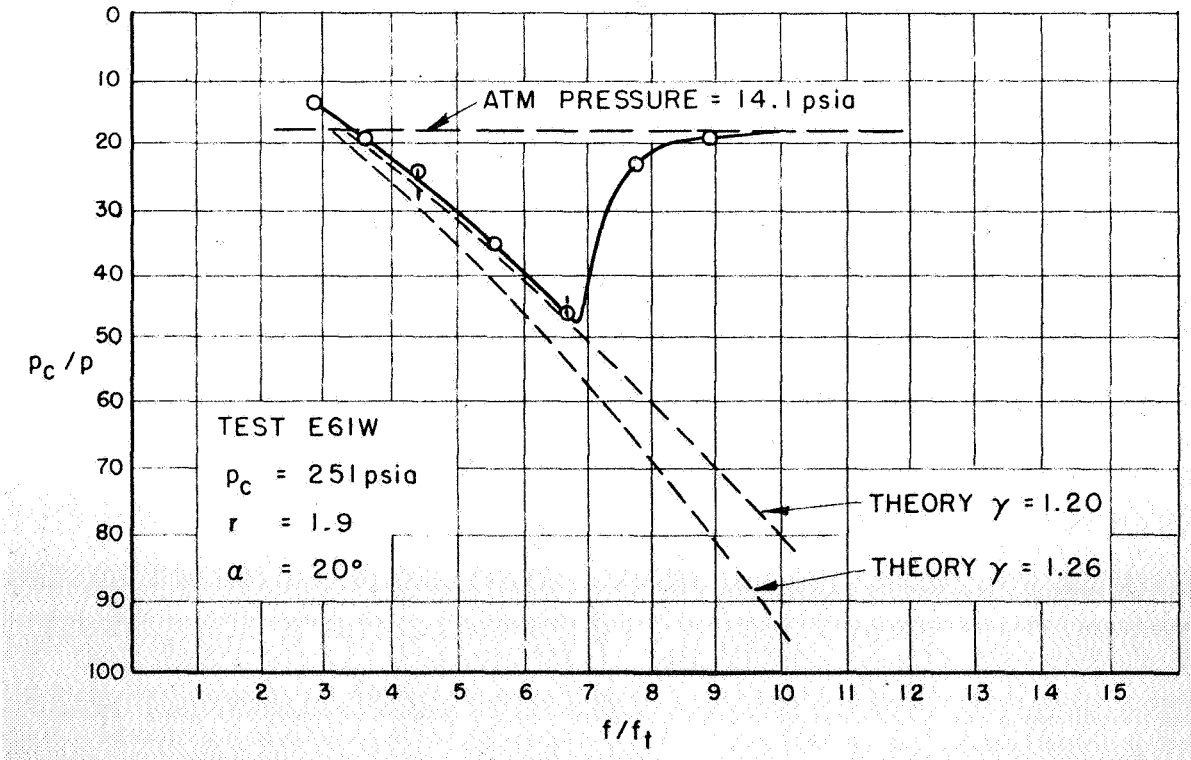

Figure 38. Pressure in Overexpanded Nozzle, ϵ = 10.0, α = 20°

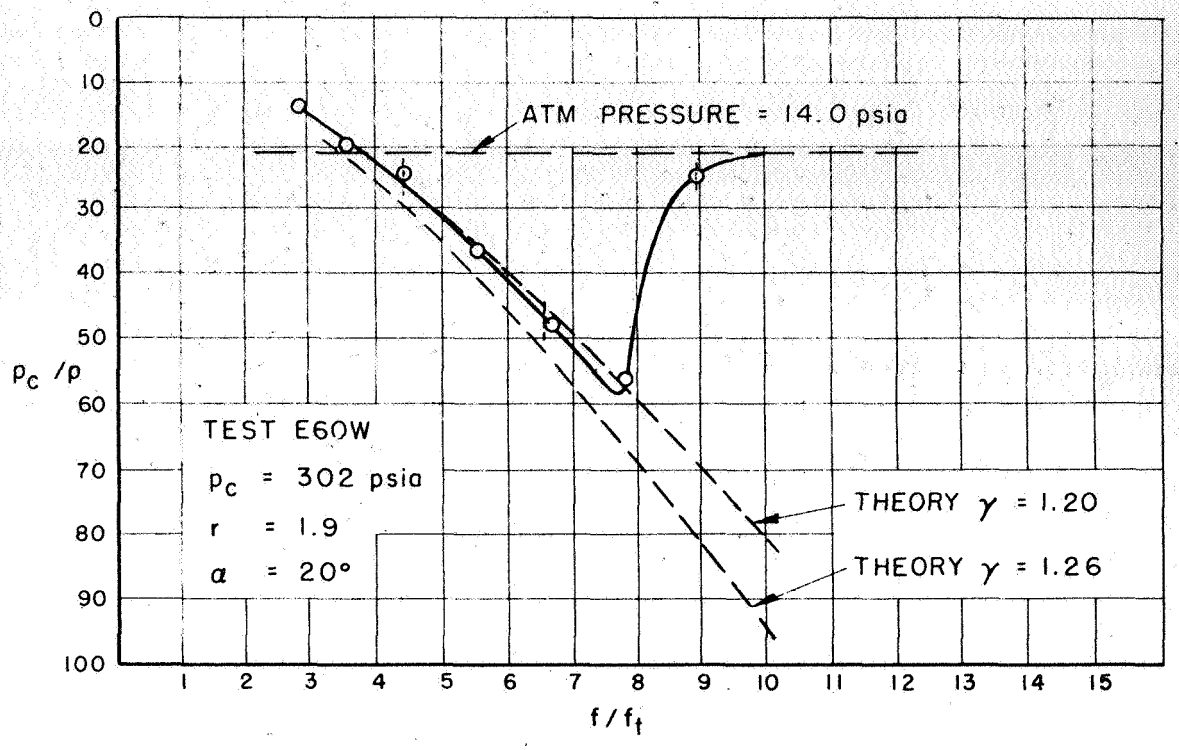

Figure 39. Pressure in Overexpanded Nozzle, $\epsilon = 10.0$, $\alpha = 20°$

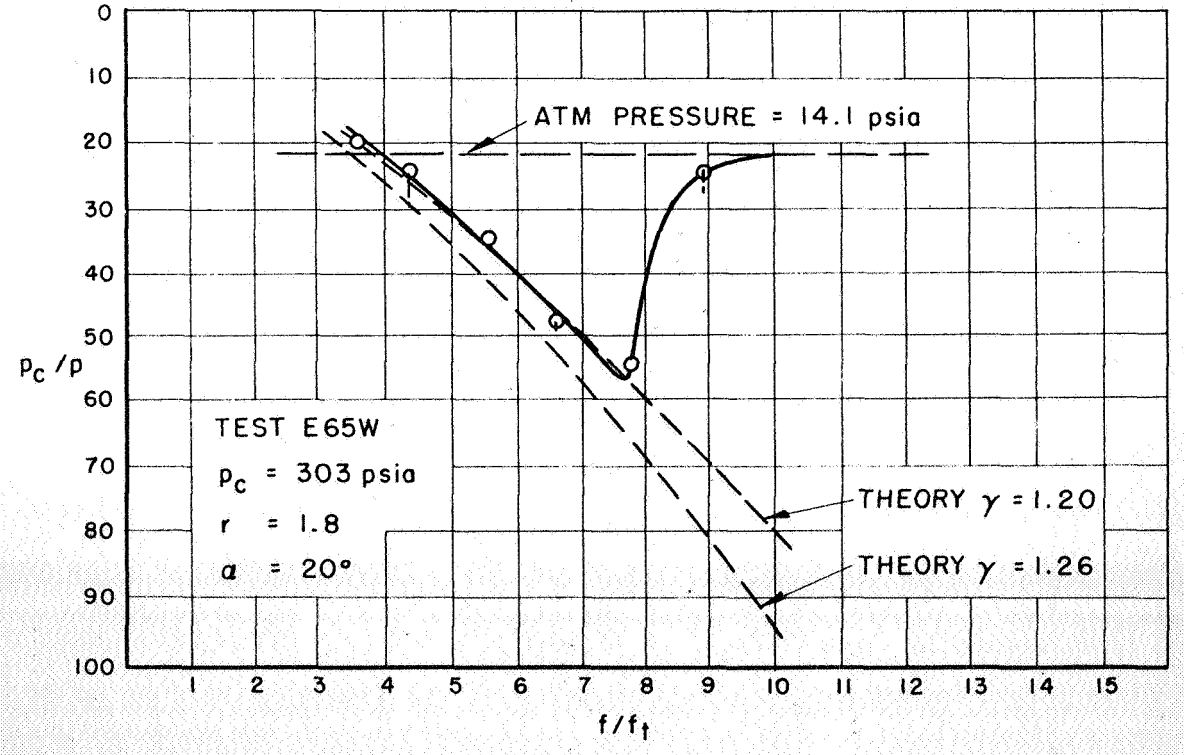

Figure 40. Pressure in Overexpanded Nozzle, $\epsilon = 10.0$, $\alpha = 20°$

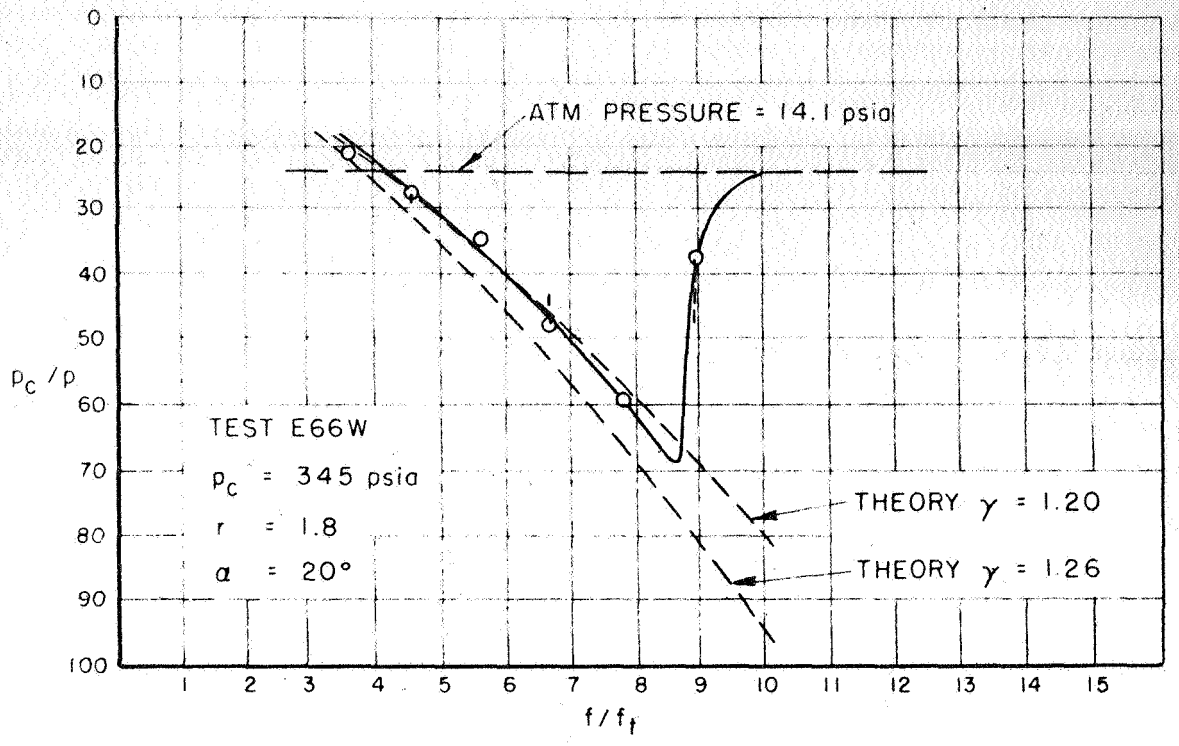

Figure 41. Pressure in Overexpanded Nozzle, ϵ = 10.0, α = 20°

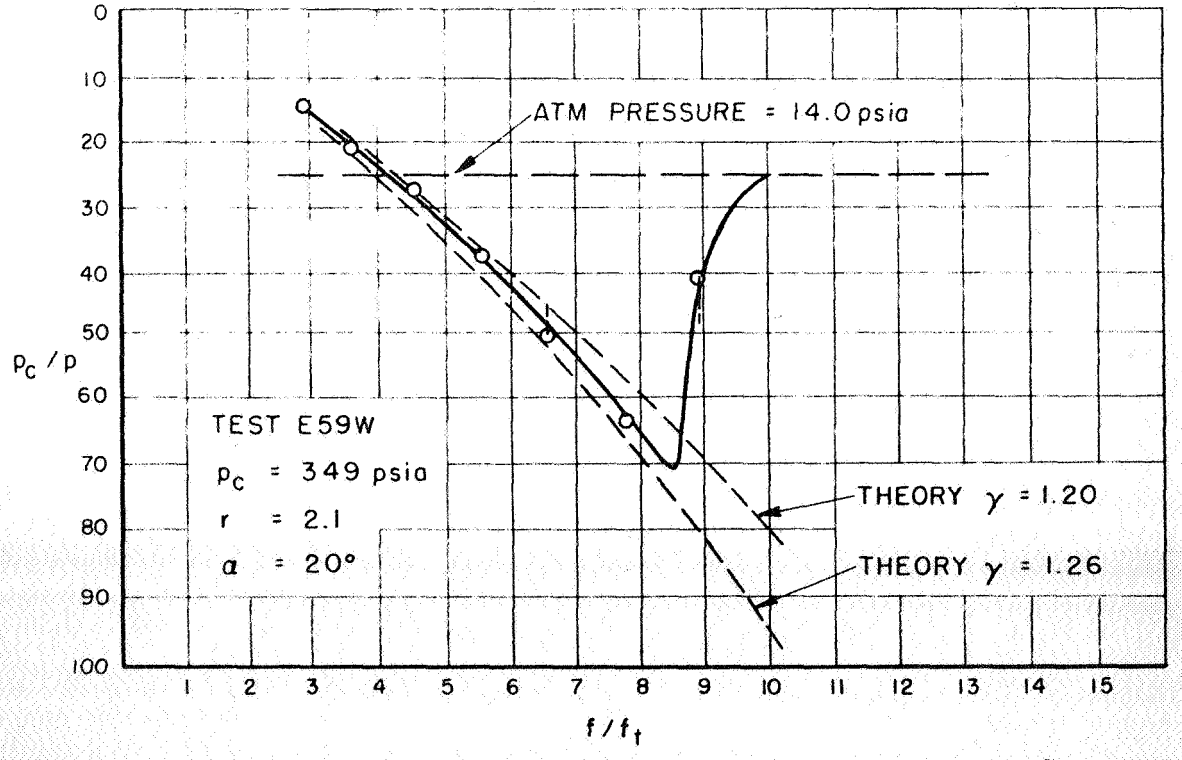

Figure 42. Pressure in Overexpanded Nozzle, ϵ = 10.0, α = 20°

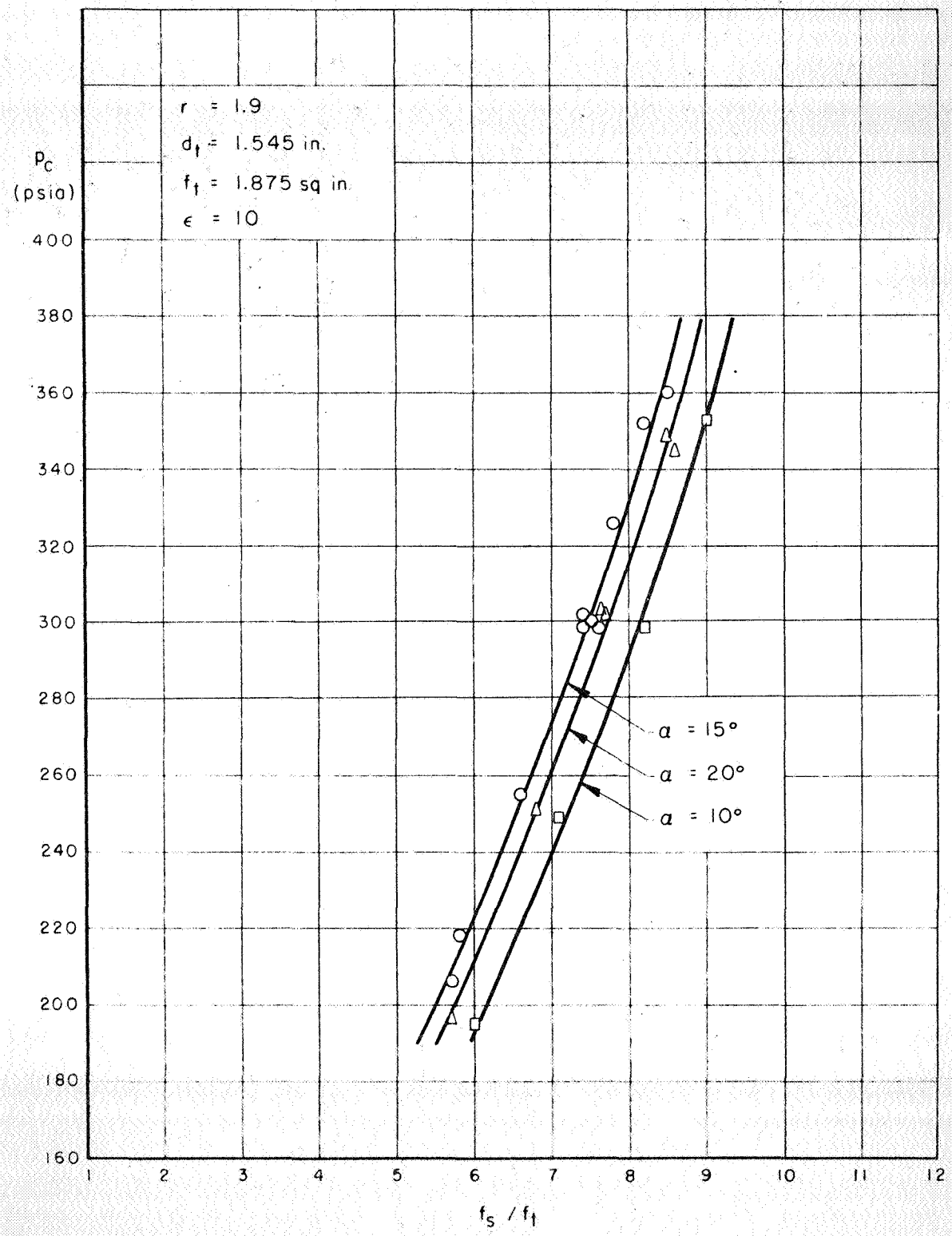

Figure 43. Area Ratio at Plane of Separation vs Chamber Pressure for ϵ = 10.0, α = 10, 15, and 20°

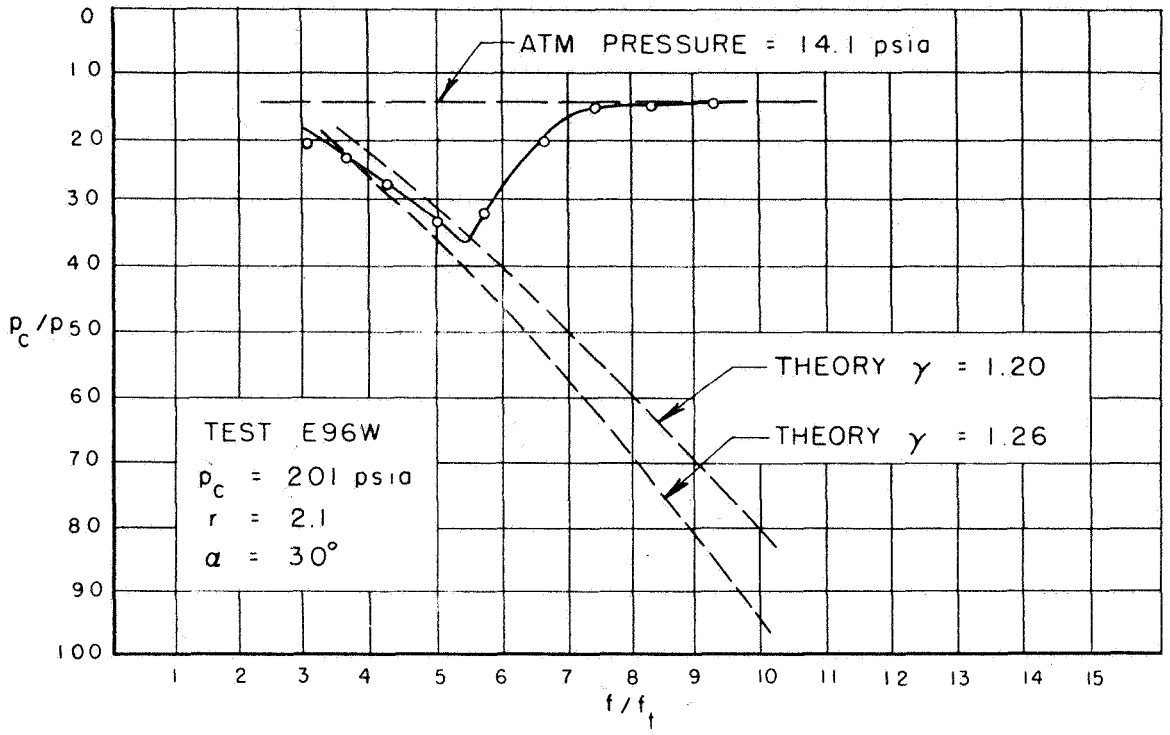

Figure 44. Pressure in Overexpanded Nozzle, ϵ = 10.0, α = 30°

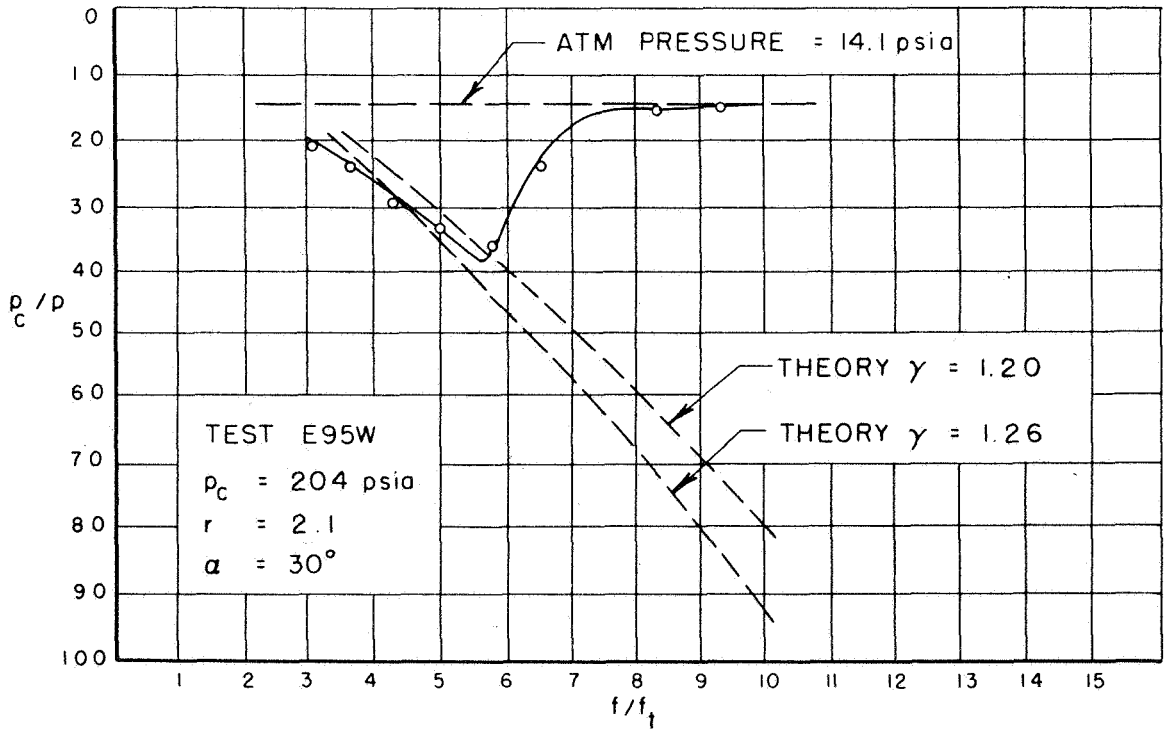

Figure 45. Pressure in Overexpanded Nozzle, ϵ = 10.0, α = 30°

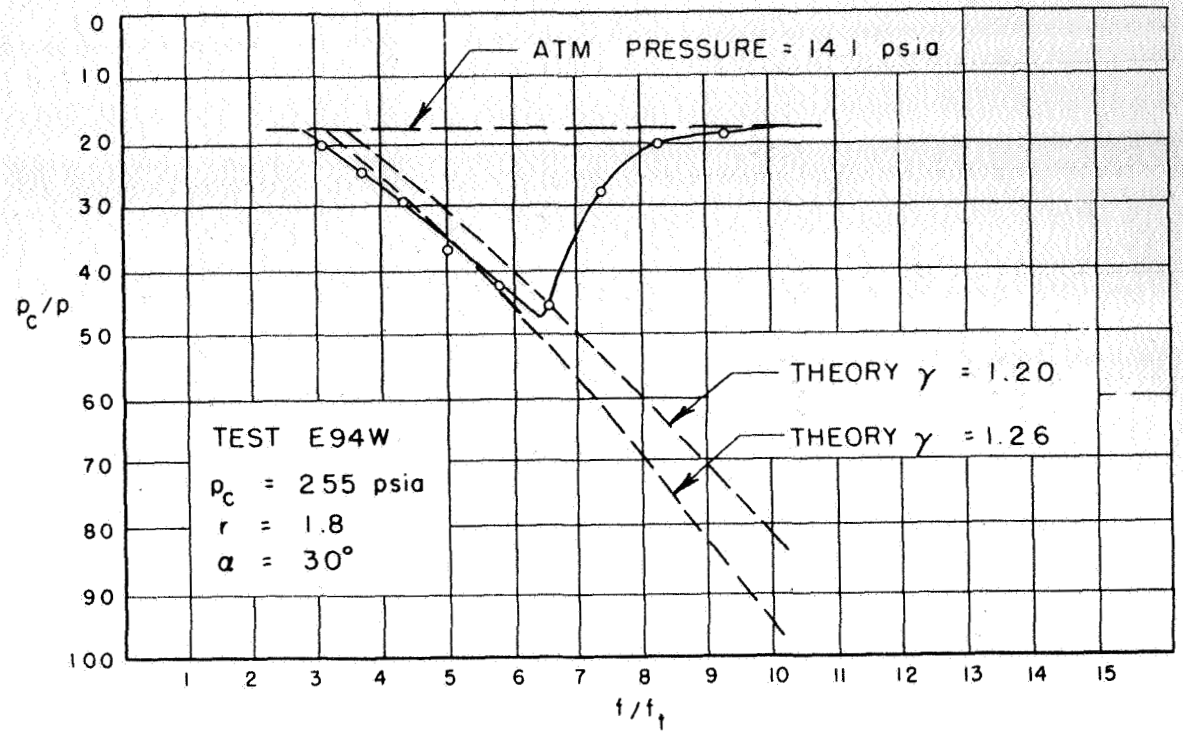

Figure 46. Pressure in Overexpanded Nozzle, $\epsilon = 10.0$, $\alpha = 30°$

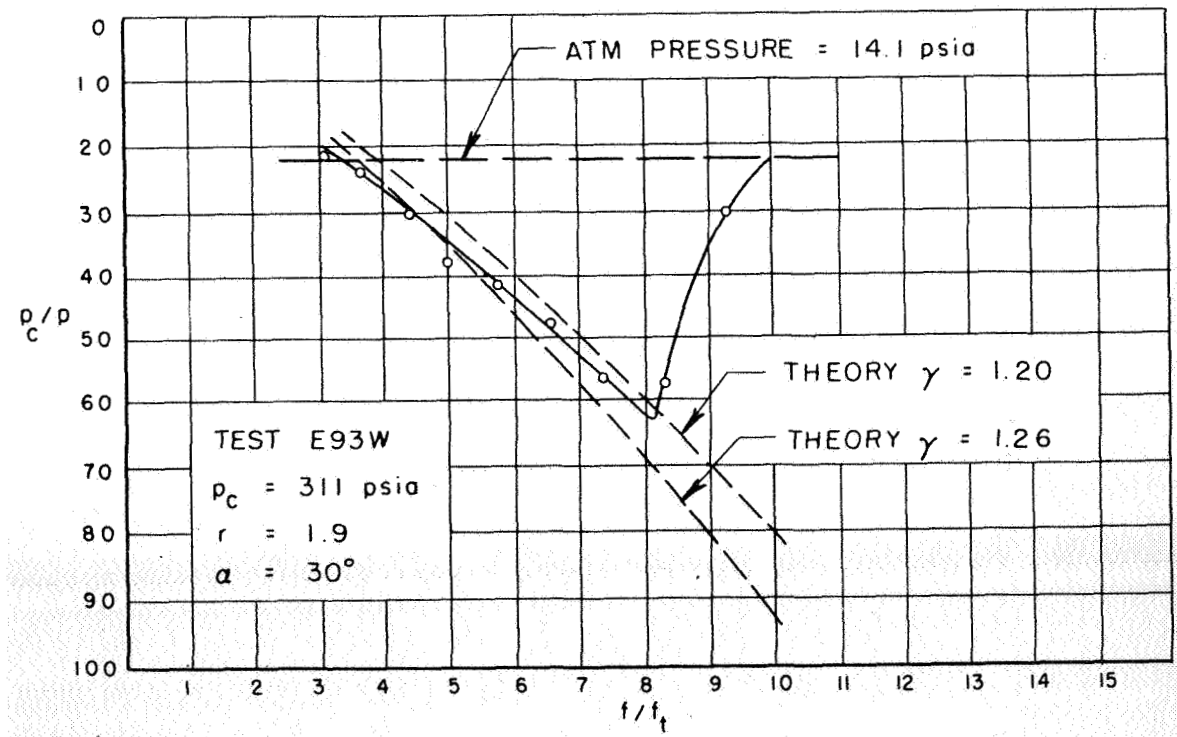

Figure 47. Pressure in Overexpanded Nozzle, $\epsilon = 10.0$, $\alpha = 30°$

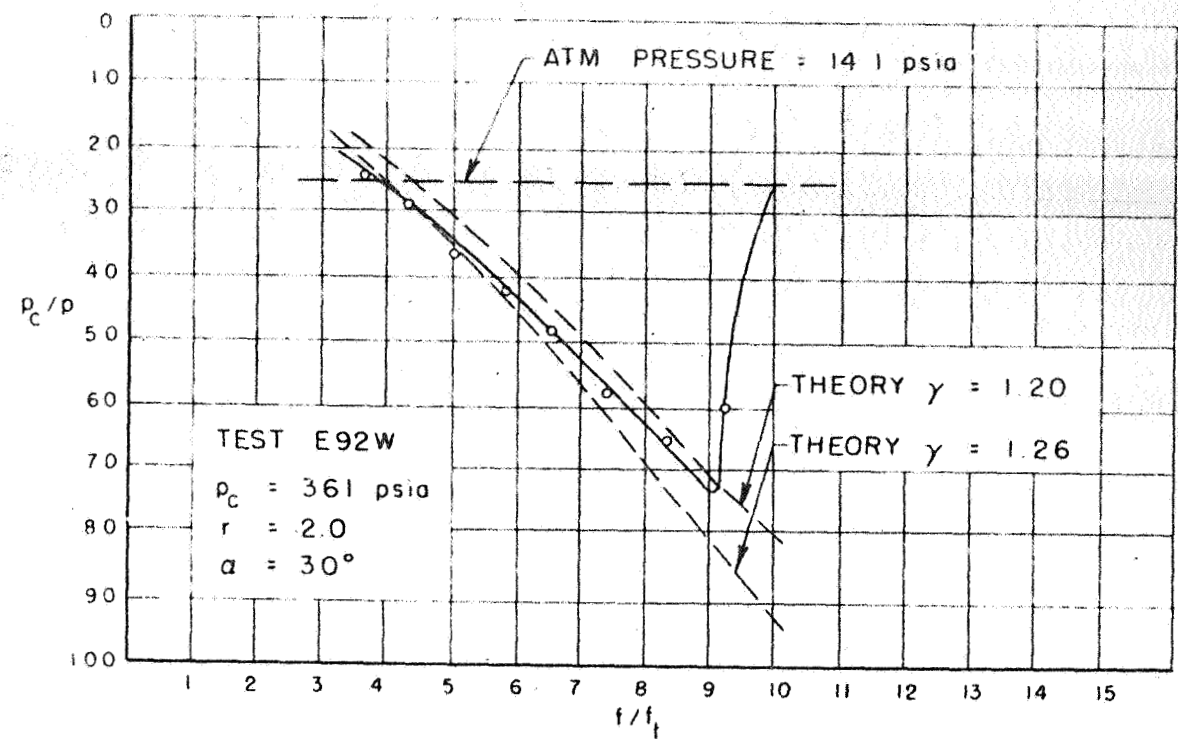

Figure 48. Pressure in Overexpanded Nozzle, $\epsilon = 10.0$, $\alpha = 30°$

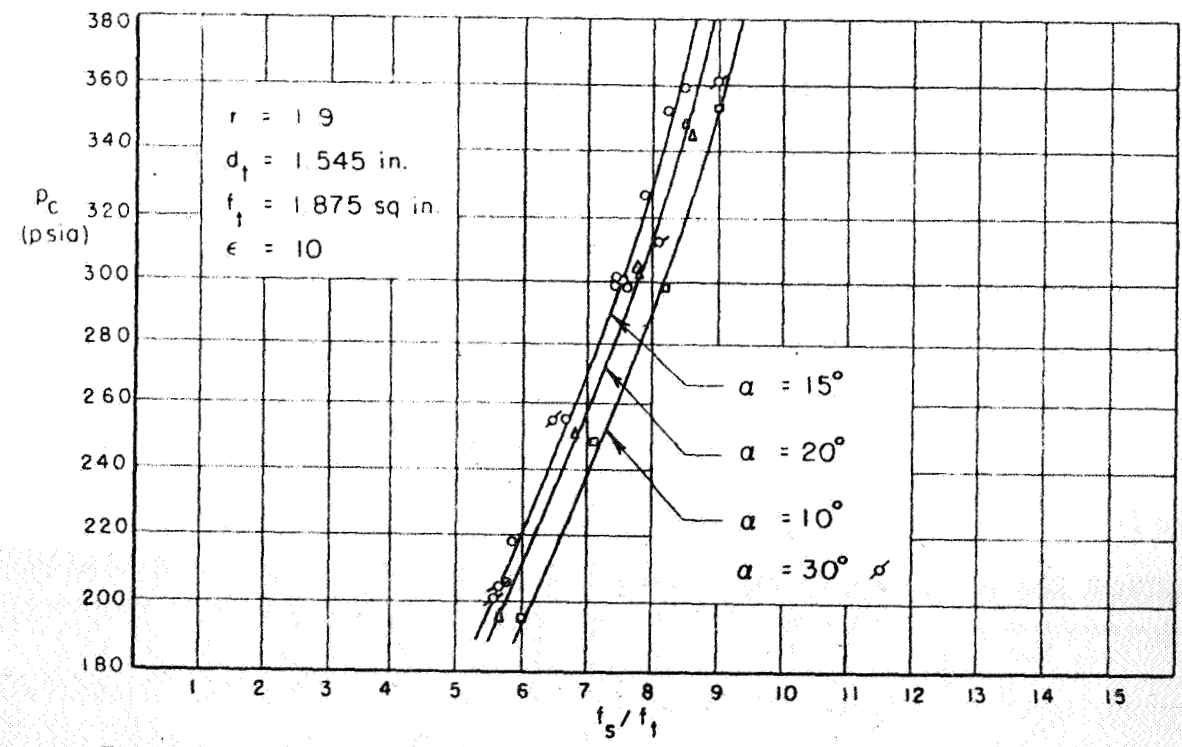

Figure 49. Area Ratio at Plane of Separation vs Chamber Pressure for $\epsilon = 10.0$, $\alpha = 10$, 15, 20, and 30°

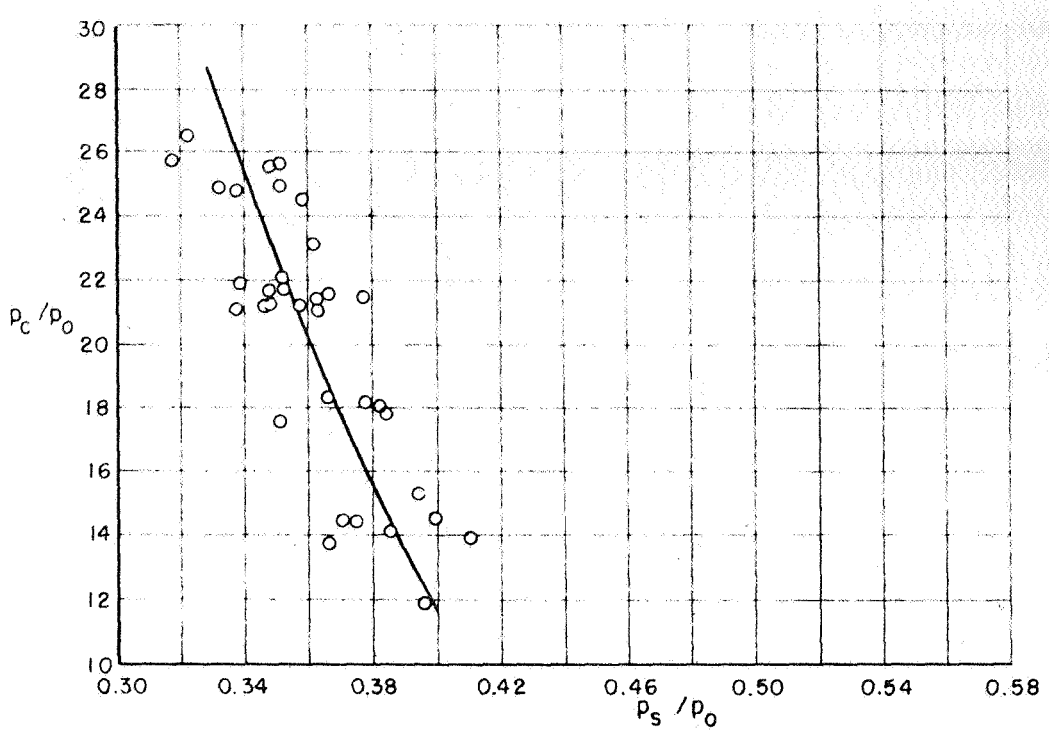

Figure 50. Variation of Separation Pressure with Chamber Pressure

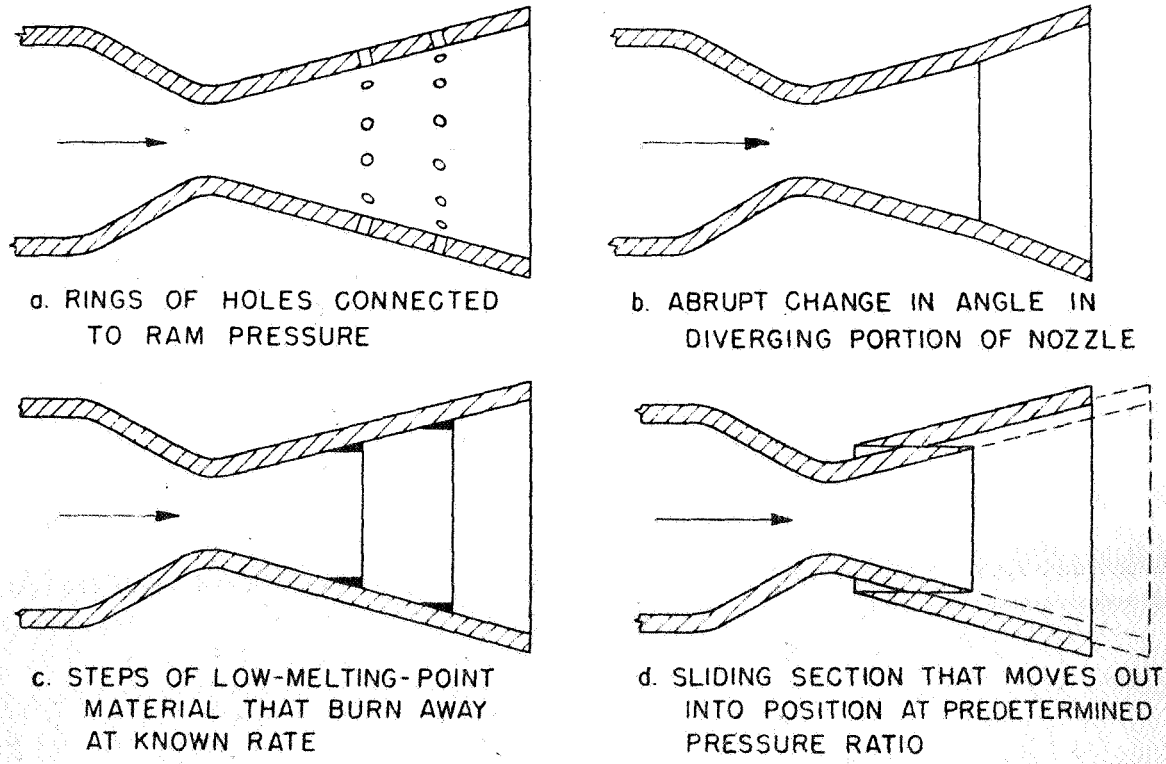

Figure 51. Possible Methods for Inducing Gas Separation

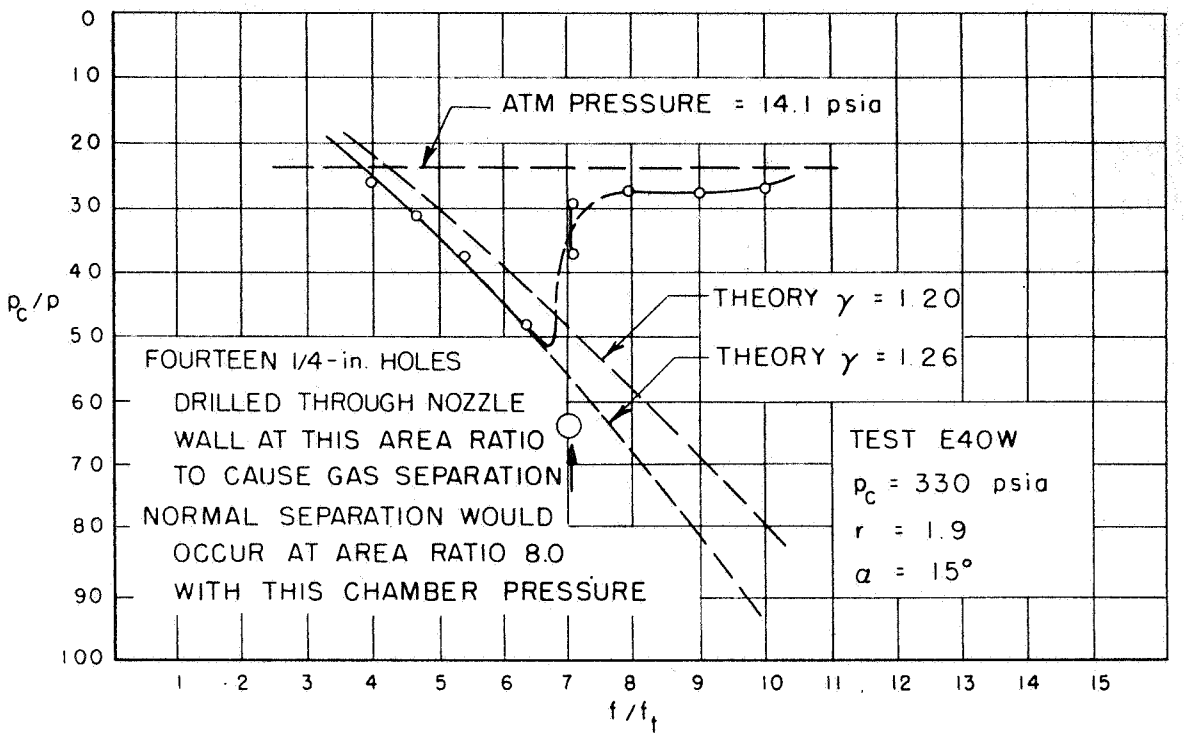

Figure 52. Tests on Inducing Gas Separation

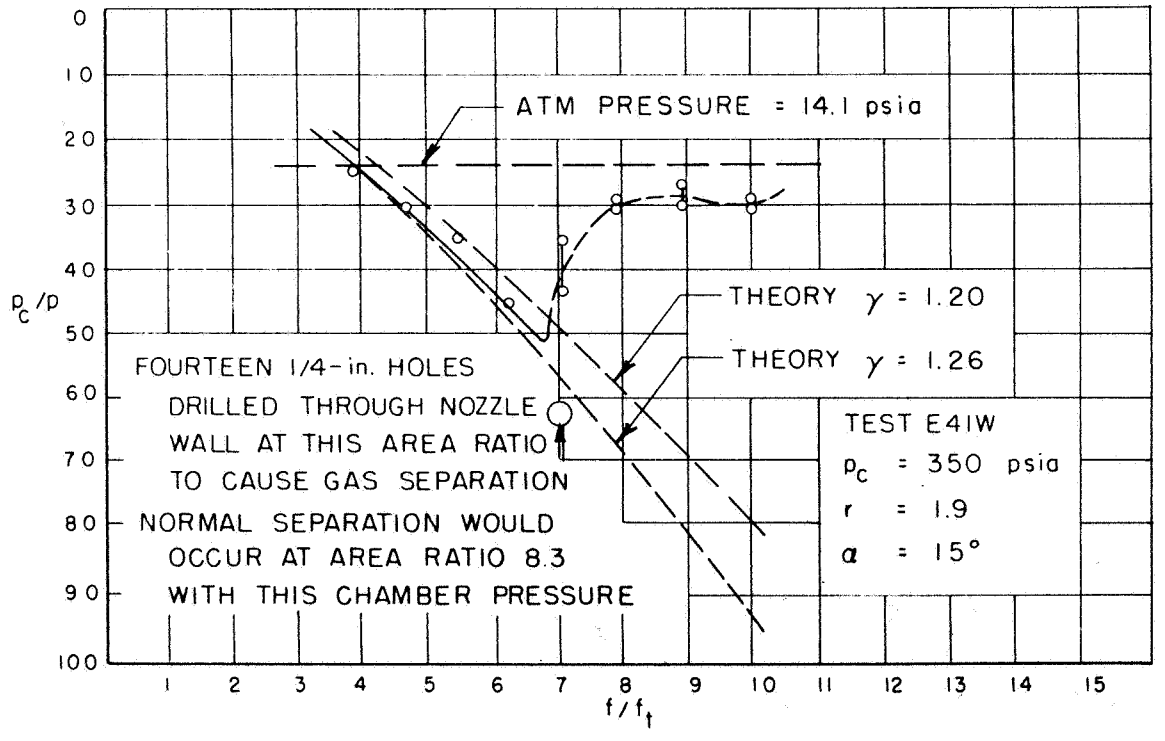

Figure 53. Tests on Inducing Gas Separation

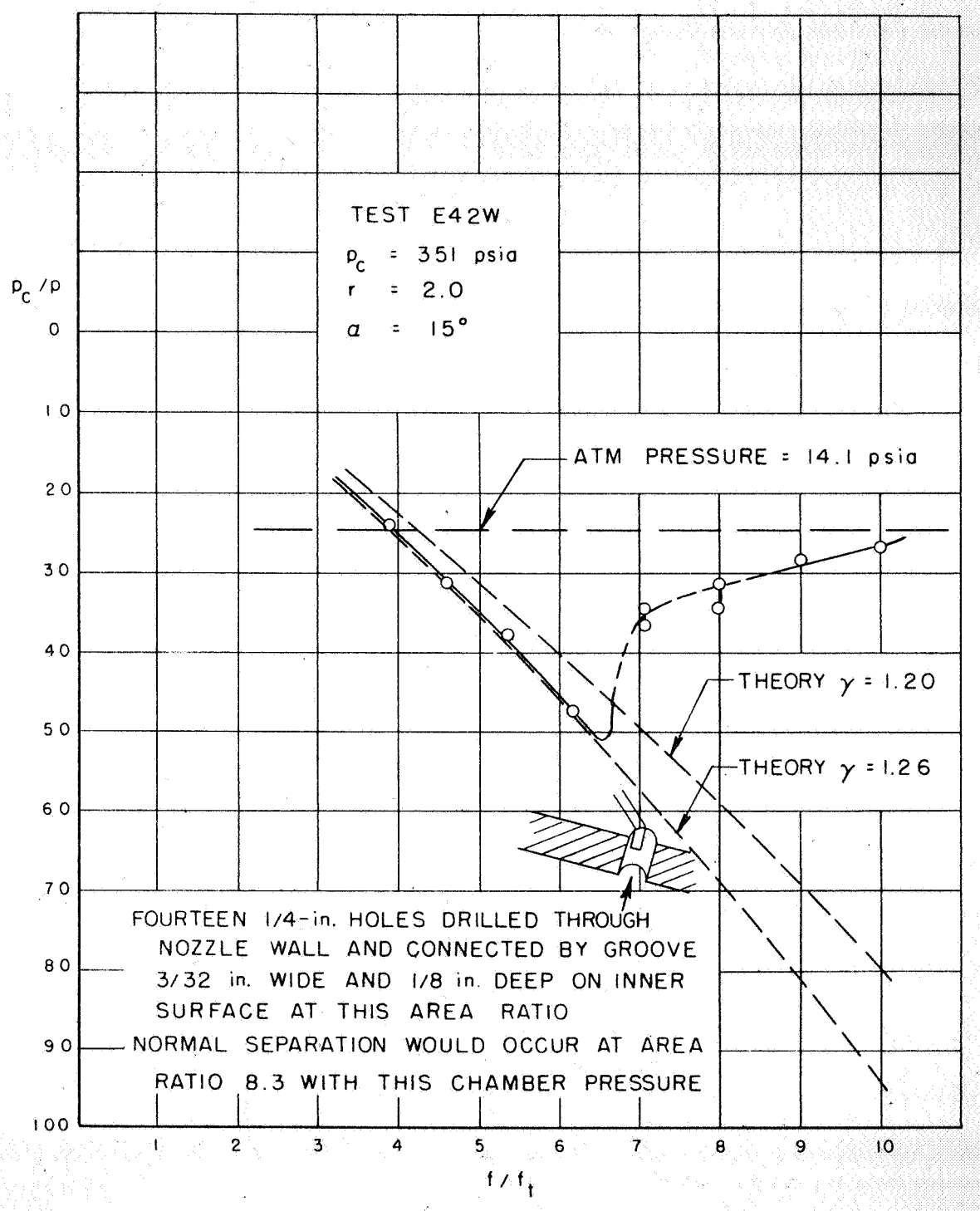

Figure 54. Tests on Inducing Gas Separation

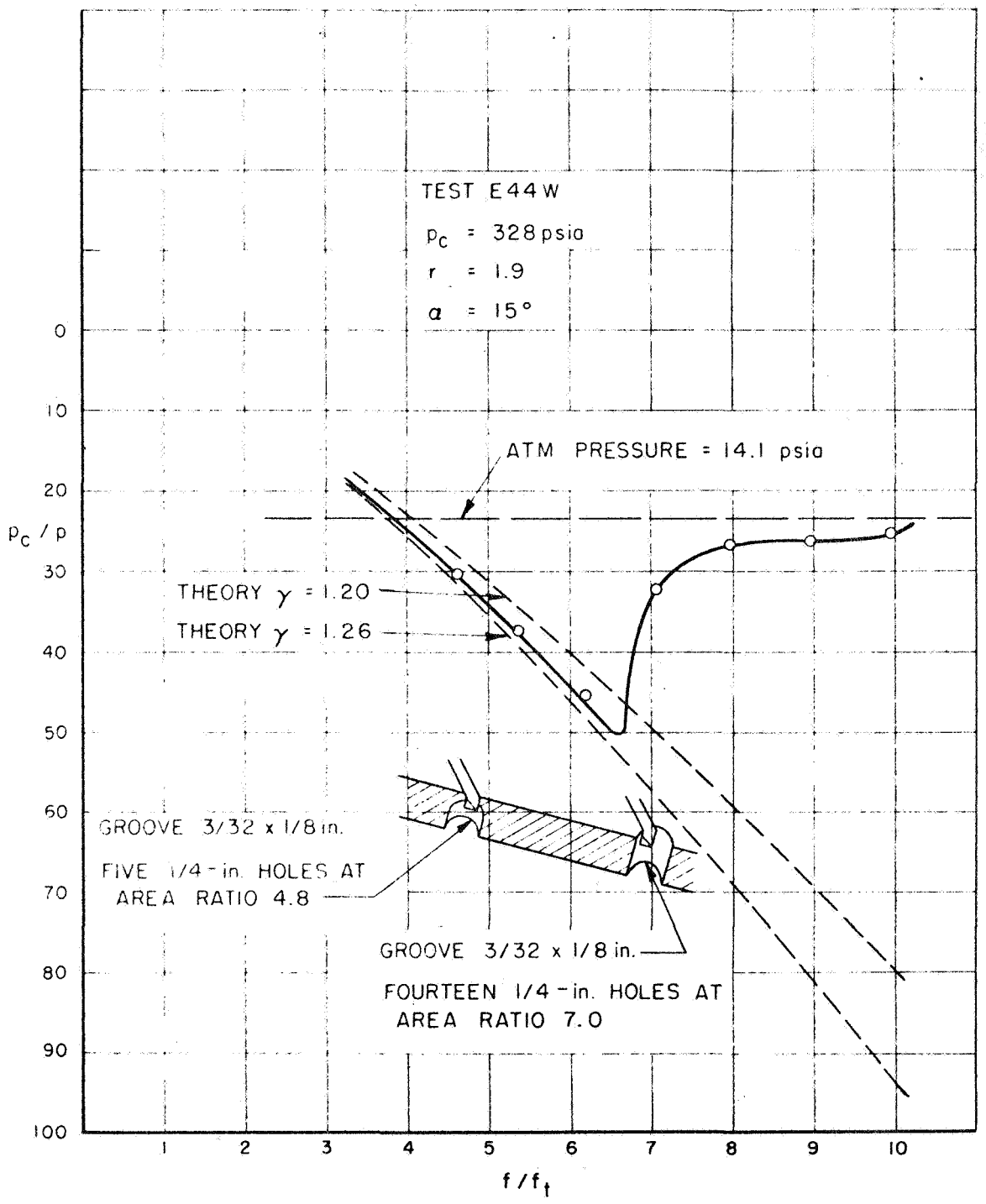

Figure 55. Tests on Inducing Gas Separation

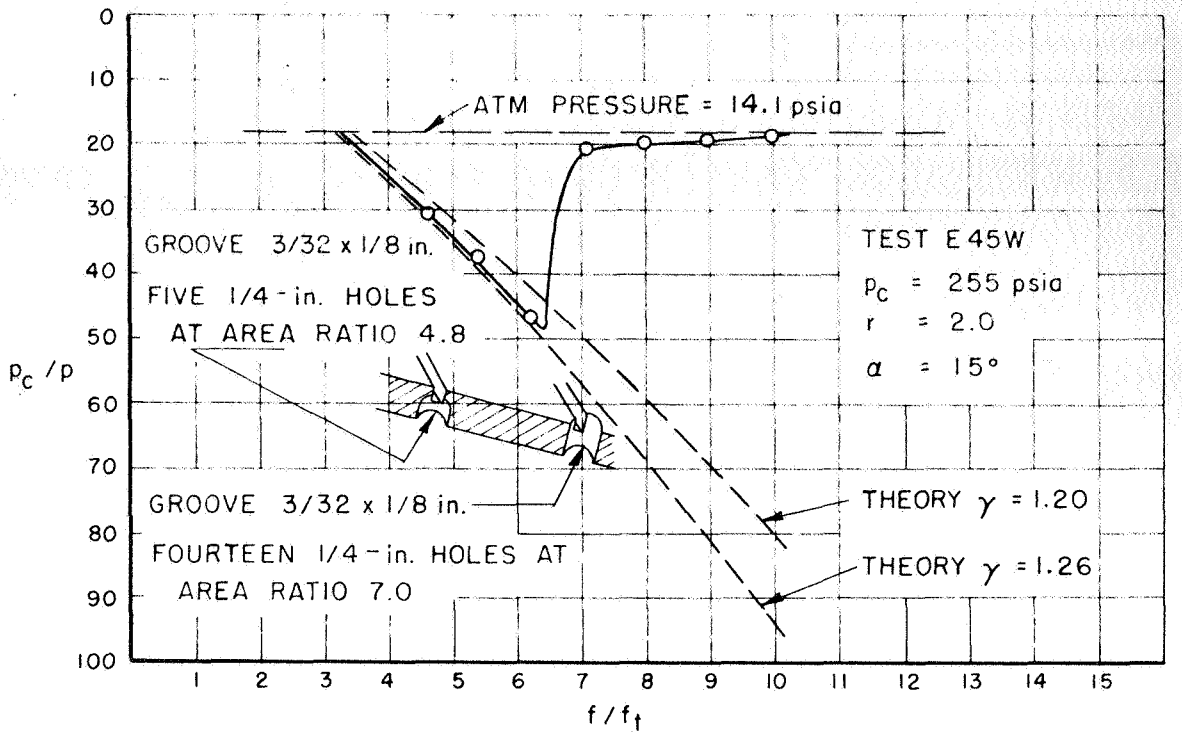

Figure 56. Tests on Inducing Gas Separation

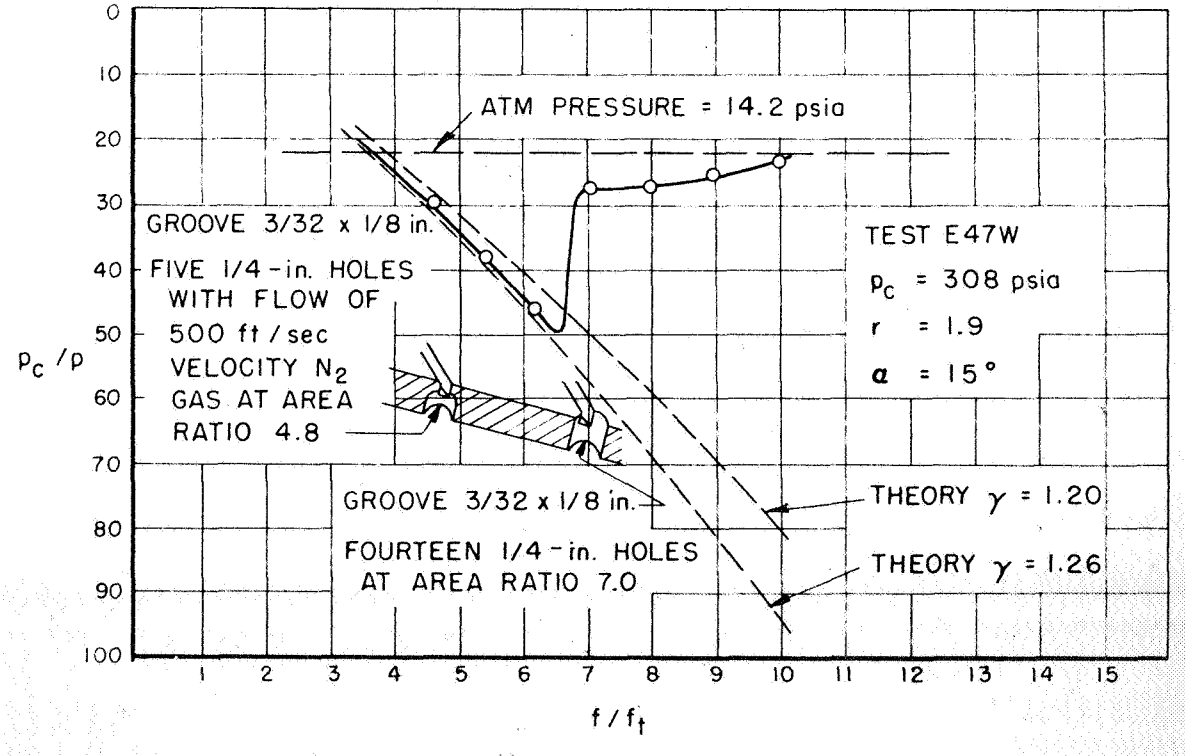

Figure 57. Tests on Inducing Gas Separation

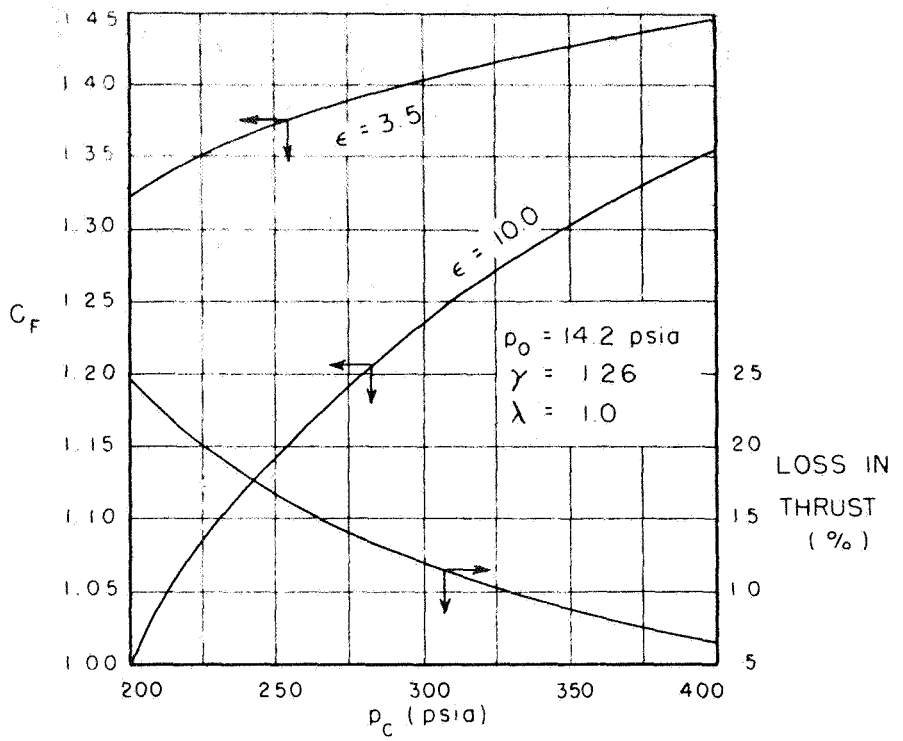

Figure 58. Theoretical Thrust Coefficient, Neglecting Separation

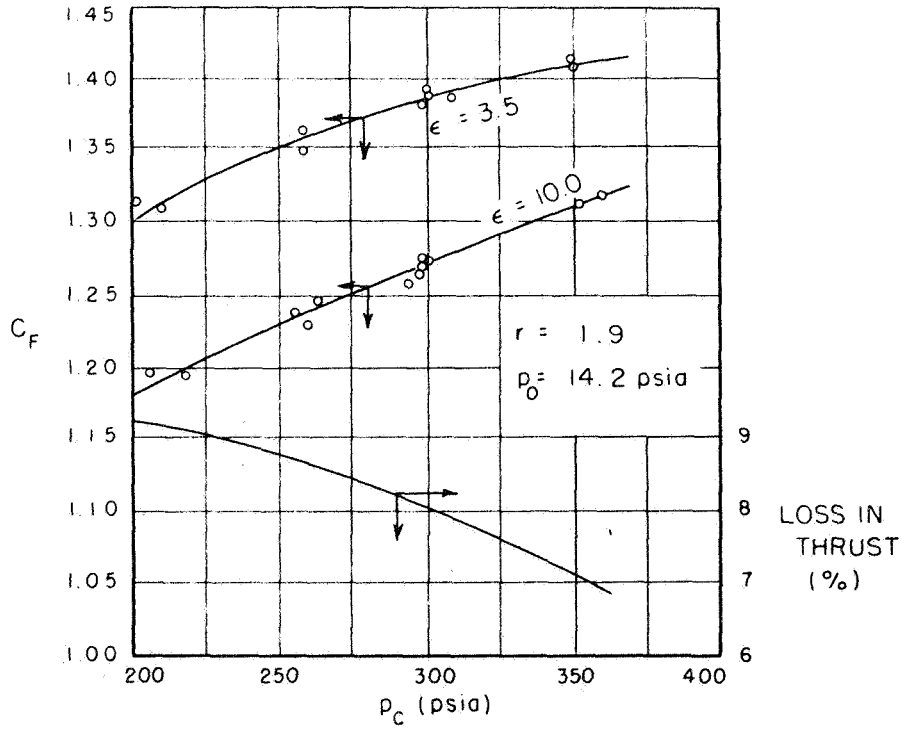

Figure 59. Experimental Thrust Coefficient, $\alpha = 15°$

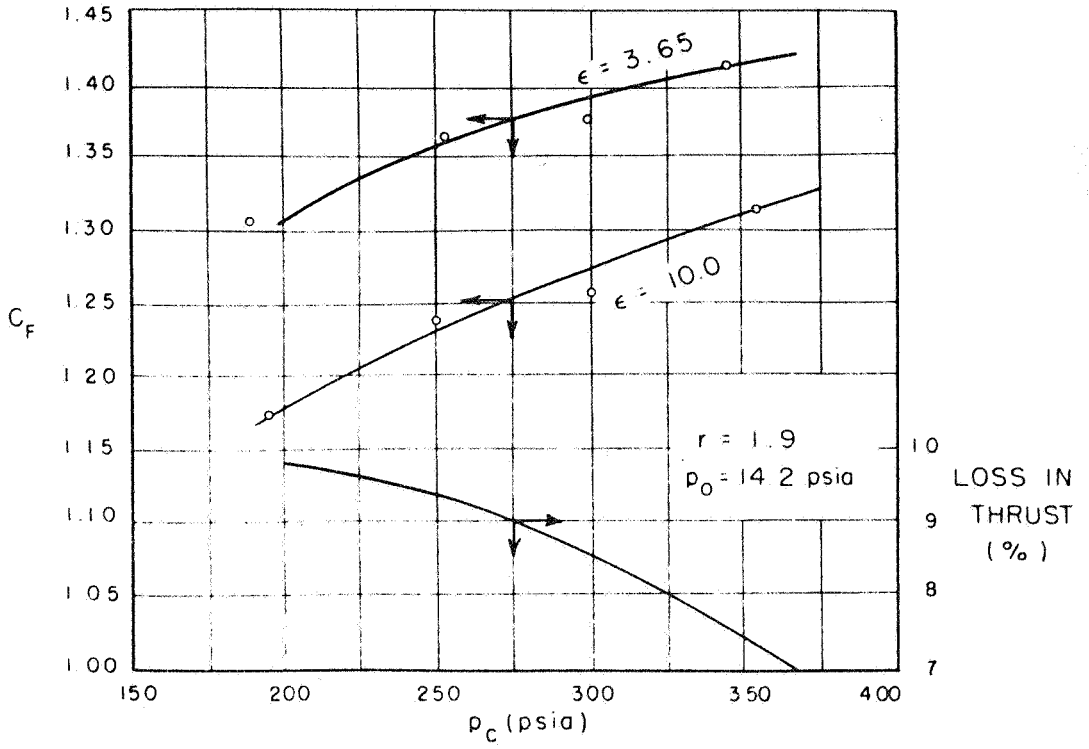

Figure 60. Experimental Thrust Coefficient, $\alpha = 10°$

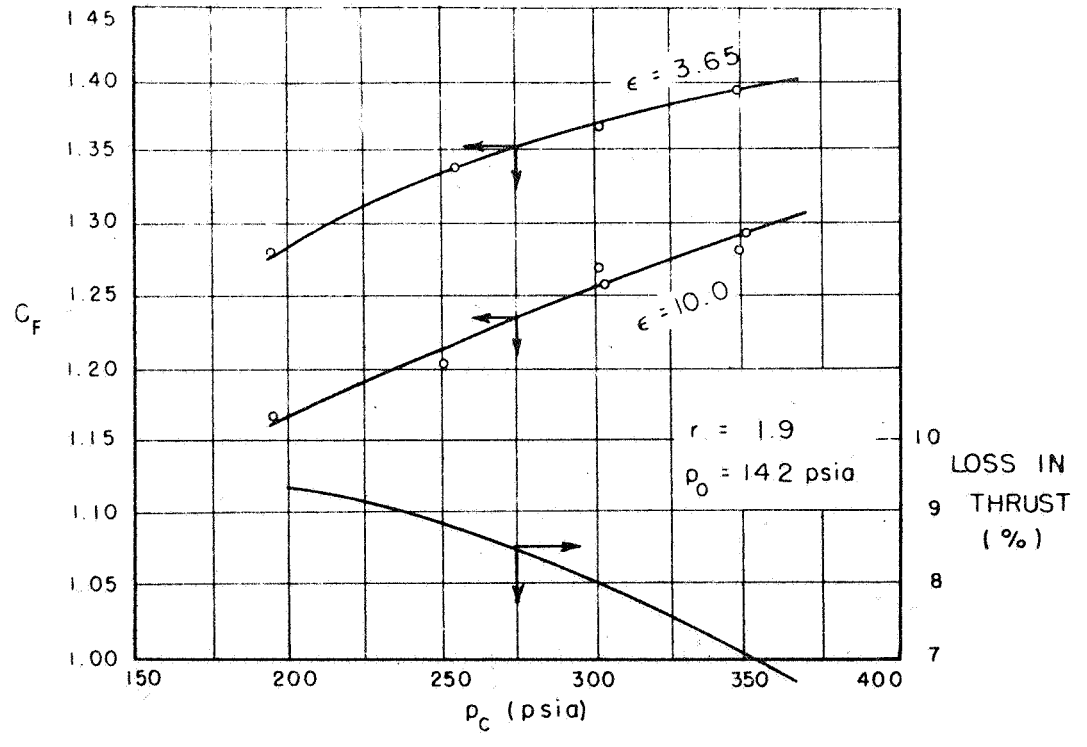

Figure 61. Experimental Thrust Coefficient, $\alpha = 20°$

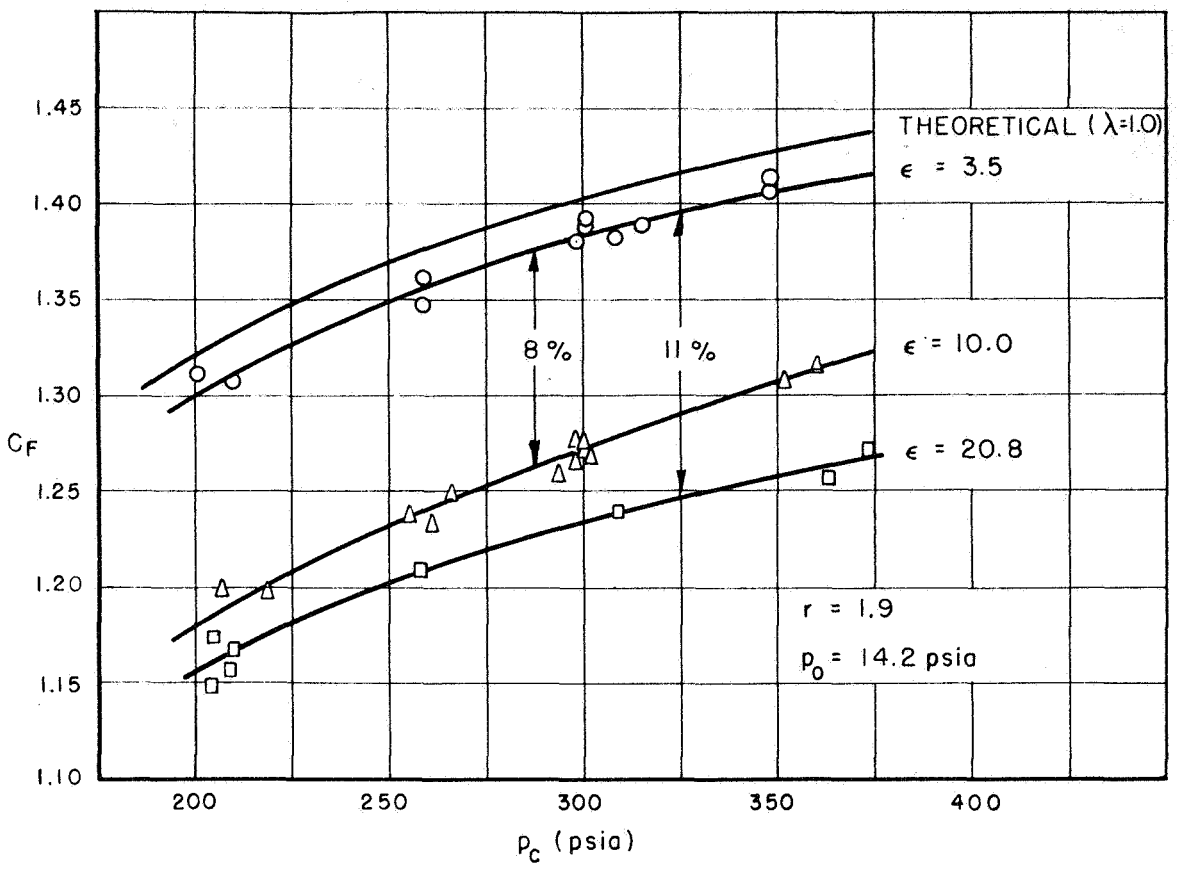

Figure 62. Experimental Thrust Coefficient, $\alpha = 15°$, $\epsilon = 3.5, 10.0, 20.8$

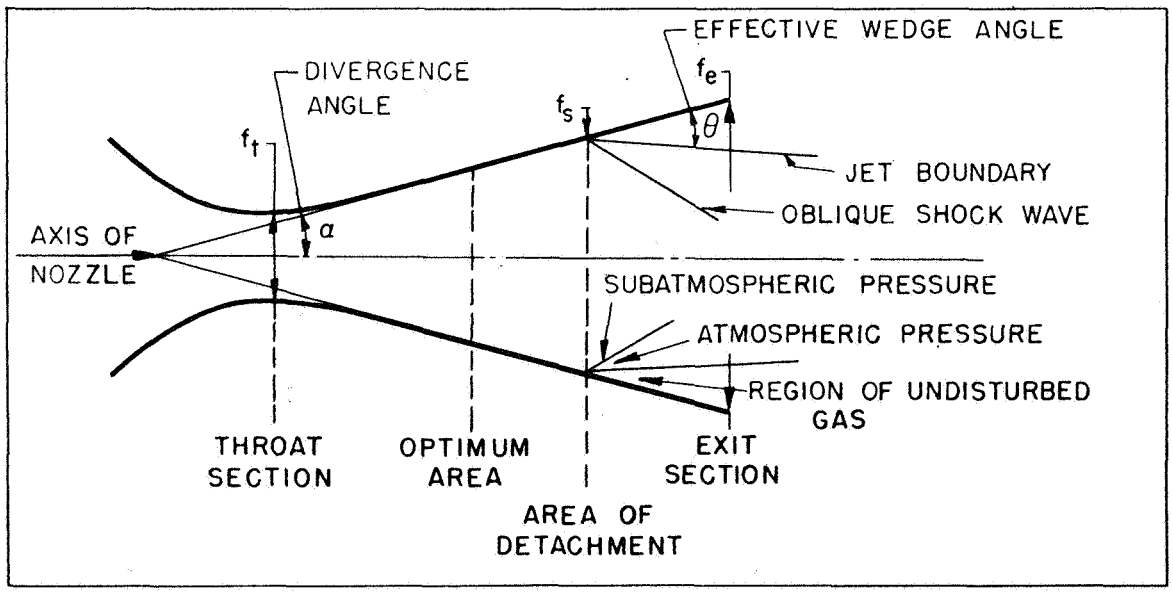

Figure 63. Hypothetical Flow Structure in Overexpanded Exhaust Nozzle

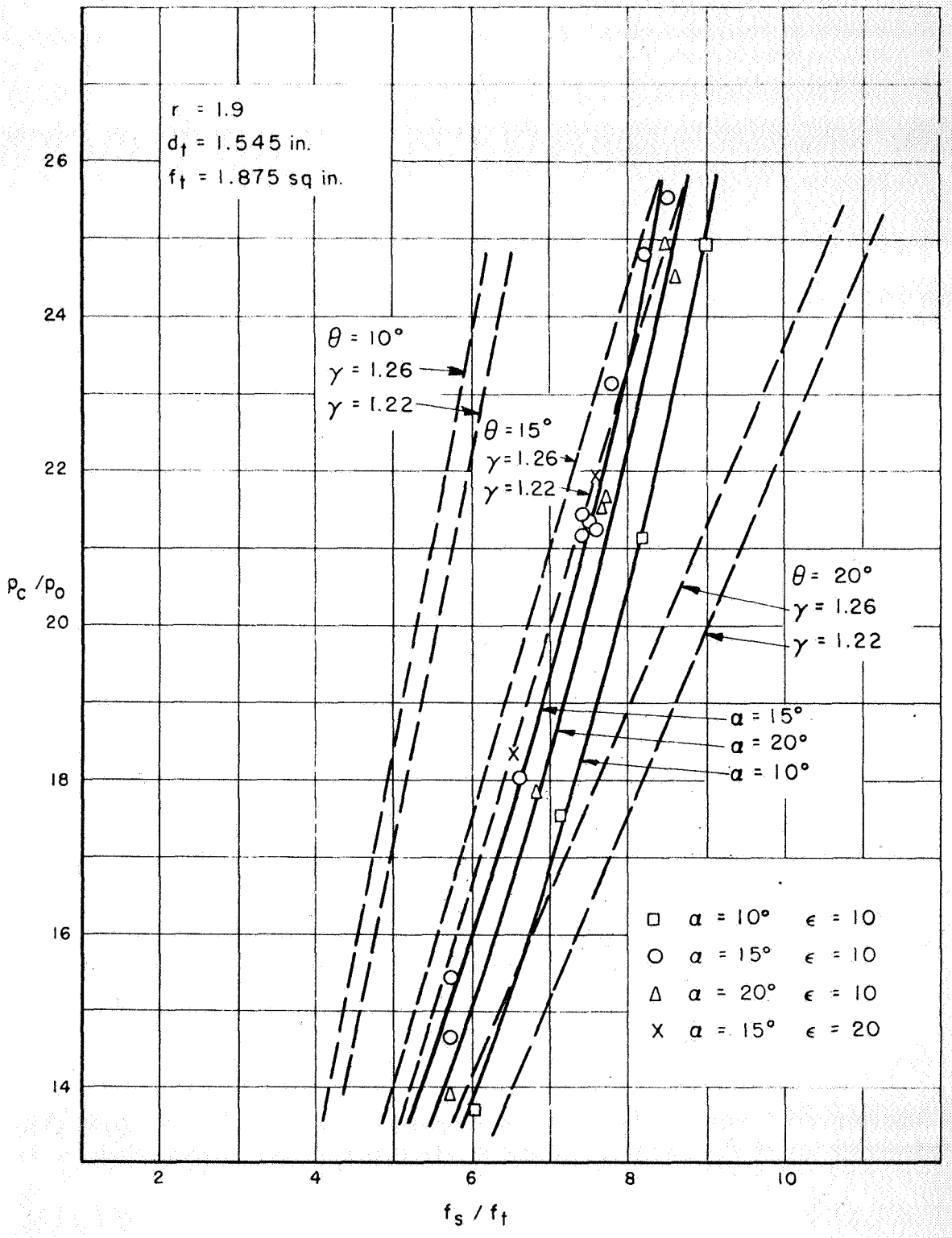

Figure 64. Variation of Plane of Gas Separation with Chamber Pressure

BLANK PAGE 48

REFERENCES

1. Seifert, Howard S., Mills, Mark M., and Summerfield, Martin, "The Physics of Rockets," *American Journal of Physics,* 15 (No. 1): 1-21, 1947.

2. Malina, F. J., "Characteristics of the Rocket Motor Unit Based on the Theory of Perfect Gases," *Journal of the Franklin Institute,* 230 (No. 4): 433-454, 1940.

3. Swan, Walter C., *The Influence of Nozzle Design on the Flight Performance of Rocket Vehicles, with an Analysis of the Results of Jet Separation* (thesis). Pasadena: California Institute of Technology, 1948.

THIS REPORT HAS BEEN DISTRIBUTED ACCORDING TO SECTIONS A, C, AND DP OF THE JOINT ARMY-NAVY-AIR FORCE MAILING LIST NO.9 DATED 1 SEPTEMBER 1949 AND CHANGE SHEET NO. 1 DATED 1 NOVEMBER 1949